Earth Syst. Sci. Data, 13, 3467–3490, 2021
https://doi.org/10.5194/essd-13-3467-2021

Open Access Earth System Science Data

A global database of marine isotope substage 5a and 5c marine terraces and paleoshoreline indicators

Schmitty B. Thompson and Jessica R. Creveling

College of Earth, Ocean, and Atmospheric Sciences, Oregon State University, Corvallis, 97331 OR, USA

Correspondence: Schmitty B. Thompson (thomschm@oregonstate.edu)

Received: 15 January 2021 – Discussion started: 1 February 2021
Revised: 7 June 2021 – Accepted: 10 June 2021 – Published: 16 July 2021

Abstract. In this review we compile and document the elevation, indicative meaning, and chronology of marine isotope substage 5a and 5c sea level indicators for 39 sites within three geographic regions: the North American Pacific coast, the North American Atlantic coast and the Caribbean, and the remaining globe. These relative sea level indicators, comprised of geomorphic indicators such as marine and coral reef terraces, eolianites, and sedimentary marine- and terrestrial-limiting facies, facilitate future investigation into marine isotope substage 5a and 5c interstadial paleo-sea level reconstruction, glacial isostatic adjustment, and Quaternary tectonic deformation. The open-access database, presented in the format of the World Atlas of Last Interglacial Shorelines (WALIS) database, can be found at https://doi.org/10.5281/zenodo.5021306 (Thompson and Creveling, 2021).

1 Introduction

Two orbitally modulated peaks in Northern Hemisphere summer insolation, occurring ~ 100 and ~ 80 ka, brought warmer temperatures and reduced ice volumes that briefly interrupted earth's transition from the last interglacial into the last glacial maximum (Hays et al., 1976; Chappell and Shackleton, 1986; Lambeck and Chappell, 2001; Cutler et al., 2003). These interstadials induced $\delta^{18}O_{benthic}$ excursions, designated as marine isotope stages (MISs) 5c and 5a, coincident with highstands in sea level inferred from uplifted reefs and shore platforms and additional sedimentological indicators (Mesolella et al., 1969; Railsback et al., 2015). Inquiry into MIS 5a and 5c sea level highstands enriches our understanding of last interglaciation (sensu lato) paleoclimate (e.g., Potter et al., 2004) and tectonic deformation (e.g., Simms et al., 2016), and faunal assemblages preserved on and within marine terraces reveal ocean paleo-temperature and paleo-circulation pathways (Muhs et al., 2012), all of which complement insight gained from the preceding MIS 5e substage (Kopp et al., 2009; Dutton and Lambeck, 2012; Dutton et al., 2015).

A rich literature catalogues the legacy of mapping globally distributed MIS 5a and 5c reef tracts, shore platforms, and other marine- and terrestrial-limiting sedimentological indicators for the purpose of measuring the local peak sea level achieved during these ice-volume minima (Griggs, 1945; Alexander, 1953; Bretz, 1960; Land et al., 1967; Mesolella, 1967; Chappell, 1974; Chappell and Veeh, 1978; Cronin et al., 1981). Here we adopt the standardized framework provided by the World Atlas of Last Interglacial Shorelines (WALIS) database (WALIS, https://warmcoasts.eu/world-atlas.html, last access: 23 June 2021) to compile the English-language publications of globally outcropping relative sea level (RSL) indicators ascribed by the primary authors as MIS 5a and 5c in age. The open-access database, which includes site descriptions, elevation and geochronological constraints, and associated metadata, is available at this link: https://doi.org/10.5281/zenodo.5021306 (Thompson and Creveling, 2021). Database field descriptors can be queried at this link: https://doi.org/10.5281/zenodo.3961543 (Rovere et al., 2020). This database builds on foundational regional syntheses of MIS 5a and 5c sea level indicators for the Atlantic coast of North America and the Caribbean (Potter and Lambeck, 2004), Pacific coast of the United States and Baja California in Mexico (Muhs et al., 2012; Simms et al., 2016), and a subset of far-field localities (Creveling et al., 2017) in compiling a global dataset of 39 sites (Fig. 1). The database includes sites excluded from previous reviews.

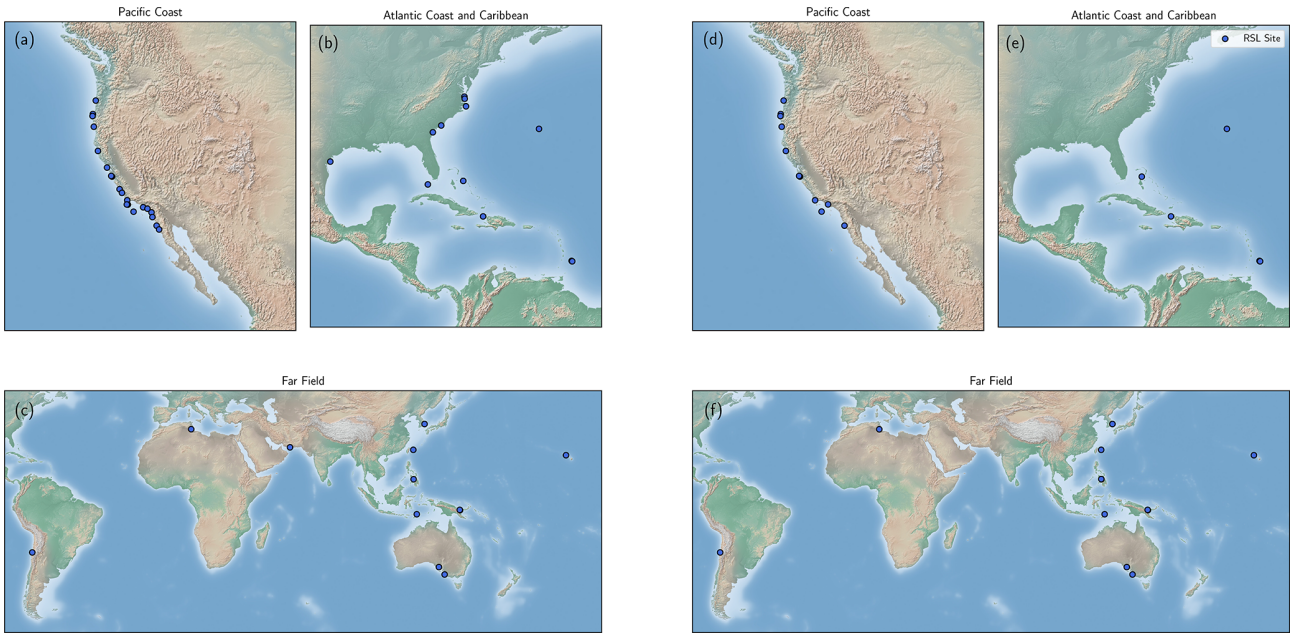

Figure 1. Locations of MIS 5a **(a–c)** and MIS 5c **(d, e)** RSL indicator sites for **(a, d)** the Pacific coast of North America, **(b, e)** Atlantic coast of North America and the Caribbean, and **(c, f)** the remaining globe atop the Matplotlib Basemap Shaded Relief map (Hunter, 2007).

The following sections include a summary of the types of geomorphic and sedimentological sea level indicators included in this review (Sect. 2); details on how elevation measurements, measurement uncertainty, and sea level data are reported (Sect. 3); and an overview of the dating methods utilized in the primary publications (Sect. 4). The majority of this publication (Sect. 5) reports the current measured elevations and chronologies, along with the history of the literature, for individual sites. Section 6 addresses the data availability. Section 7 summarizes future research directions.

The present elevation of MIS 5a and 5c sea level indicators reflects a number of convolved processes, including, but not limited to, tectonic deformation and glacial isostatic adjustment (GIA), which require carefully applied corrections to reconstruct peak global mean sea level (GMSL). Tectonic deformation can alter the elevation of an indicator by tens to hundreds of meters (Alexander, 1953; Chappell, 1974) and glacial isostatic adjustment by similar magnitudes (Creveling et al., 2015; Simms et al., 2016). For active margins, this convolution serves as an opportunity to constrain rates of Quaternary tectonic deformation (Adams, 1984; Marquardt et al., 2004; Muhs et al., 2014) given robust assumptions of the magnitude and source of MIS 5e ice-volume melt and glacial isostatic adjustment (Broecker et al., 1968; Dodge et al., 1983; Chappell and Shackleton, 1986; Creveling et al., 2015; Simms et al., 2016). Similarly after correction for tectonic uplift, discrepancies in the local elevation of globally distributed MIS 5a and 5c indicators of peak sea level retain a meaningful signal of glacial isostatic adjustment (Potter and Lambeck, 2004), which, in turn, allows for the reconstruction of peak global mean sea level and assessments of the sensitivity of Quaternary ice sheets to the influence of Milankovitch forcing on climate over sub-100 kyr timescales (Lambeck and Chappell, 2001; Potter and Lambeck, 2004; Potter et al., 2004; Muhs et al., 2012; Simms et al., 2016; Creveling et al., 2017). We emphasize that this database reports measurements of uncorrected, present-day elevation of various relative sea level indicators that will enable the user to apply corrections based on the most current data- and model-based predictions.

2 Sea level indicators

The data detailed in this review (and the associated database) comprise a set of geomorphic and sedimentological indicators of past sea level, for which a comprehensive overview can be found in Rovere et al. (2016). Marine platforms make up the largest portion of these data, particularly for the North American Pacific coast (see Muhs et al., 1992b, for a detailed description of this indicator). Constructional coral reef terraces are prevalent across the North American Atlantic coast, the Caribbean, and the far-field regions (see Chappell, 1974, for an example of this indicator). Additional sedimentary features, such as eolianites, submerged beach ridges, and exposure surfaces, make up the remainder of the local inferences.

3 Elevation measurements

Here we catalogue the elevation, with uncertainty (if listed), of a given indicator as reported in the primary publication(s) without modification. Methods adopted to measure the present-day elevation range of reported indicators vary from hand level and altimeter surveys to mapping with modern differential GPS and digital elevation models. The majority of publications summarized herein did not report the sea level datum that the elevation references, and, thus, these methods are reported in the WALIS database as "Not Reported". For those sites for which primarily field workers did not report elevation uncertainty, we noted this absence in the database and assigned a measurement uncertainty based upon the defined accuracy of the elevation measurement method. When available in the original publication, latitude and longitude coordinates for indicator sites are reproduced for the WALIS database; when unavailable, coordinates were interpreted from publication maps using Google Earth and noted accordingly.

For each site we rated the quality of the RSL elevation data following criteria established by the World Atlas of Last Interglacial Shorelines project documentation (see Relative Sea Level at https://doi.org/10.5281/zenodo.3961544). Quality assessments for RSL elevation reflect a combination of measurement precision, the specificity of the reference datum for the elevation, and the range of and uncertainty in the indicative meaning (sensu Rovere et al., 2016). When these three variables constrain total RSL uncertainty to < 1 or 1–2 m, then WALIS defines the RSL elevation quality as excellent (5) or good (4), respectively. If, however, uncertainties in these three variables lead to an RSL elevation of 2–3 or > 3 m, then a rating of average (3) or poor (2) applies, respectively. For sites without a specified reference datum (e.g., 3 m below sea level rather than 3 m below mean high tide), we limited the maximum quality rating to 3 and assigned a rating based on the remaining factors. Any RSL indicator of poorer quality than described above receives a very poor quality rating (1). Any terrestrial- or marine-limiting indicator that serves only as an upper or lower bound on RSL receives a rating of rejected (0). Not all primary references report the indicative meaning of an RSL indicator, and thus for a subset of sites we calculated the indicative meaning with the IMCalc software (Lorscheid and Rovere, 2019) in order to assign an elevation quality rating.

4 Dating techniques

Age assignments for MIS 5a and 5c sea level indicators arise from a wide variety of radiometric and non-traditional geochronologic methods. Numeric chronologies for indicators composed of in situ carbonate utilize uranium-series dating (Barnes et al., 1956; Broecker and Thurber, 1965; Osmond et al., 1965; Thurber et al., 1965; Muhs et al., 2002; 2012). Sediment-mantling sea level indicators can also yield numeric chronologies through luminescence dating (Duller, 2004; Grove et al., 2010). Amino acid racemization (AAR) creates relative chronologies, especially in conjunction with other amino acid ratios from sea level indicators benchmarked by radiometric ages (Mitterer, 1974; Miller et al., 1979; Kennedy et al., 1982). Stratigraphic relationships between adjacent sea level indicators have been extensively used to develop relative chronologies for sea level indicators, especially for sites with marine terrace sequences consisting of adjacent MIS 5e, 5c, and 5a terraces (Adams, 1984; Merritts and Bull, 1989; McInnely and Kelsey, 1990). Other sparingly used dating methods for MIS 5a and 5c indicators include electron spin resonance (ESR) (Mirecki et al., 1995), terrestrial cosmogenic nuclide dating (Perg et al., 2001), protactinium-231 dating, (Edwards et al.,1997), paleomagnetic stratigraphy (see sources discussed in Choi et al., 2008), soil development stages (Kelsey et al., 1996), radiocarbon dating (Hanson et al., 1992), and geomorphic models (Hanks et al., 1984; Valensise and Ward, 1991).

For each site we rated the quality of the RSL chronology following criteria established by the World Atlas of Last Interglacial Shorelines project documentation (see Relative Sea Level at https://doi.org/10.5281/zenodo.3961544). Quality assessment of indicator age reflects how well the geochronology translates to a stage vs. substage assignment. An excellent rating (5) attributes an RSL indicator to a narrow window within a substage of MIS 5, whereas a good rating (4) more generally assigns an RSL indicator to a substage. If geochronology only assigns an indicator to a generic interglacial (such as MIS 5), then this warrants an average rating (3). A poor rating (2) applies to incomplete chronologic data or data that provide only a minimum or maximum age on the RSL indicator. Conflicting age assignments between marine isotope stages warrant a very poor quality rating (1). Finally, chronologic data unable to distinguish between two or more Pleistocene epoch interglacials warrant a rejected quality rating (0).

5 A global database of marine isotope substage 5a and 5c relative sea level indicators

5.1 North American Pacific coast

Field observers first documented emergent marine terraces on the North American Pacific coast in the early 20th century. Early mapping efforts documented terraces along much of the California coastline (Ellis, 1919; Davis, 1932; Woodring et al., 1946). Alexander (1953) pioneered the interpretation of west coast marine terraces as indicators of paleo-sea level and tectonic uplift. Since then, extensive documentation of regional MIS 5a and 5c paleo-sea level indicators has yielded 18 sites, which are included in the present review. As noted below, many such studies reported geomorphic or chronological data that apply to multiple adjacent sites. Griggs (1945) completed early work on the Oregon coast, documenting four

terraces, of which we focus on the Whisky Run and Pioneer terraces. McInelly and Kelsey (1990) provided further geomorphic cross-sections for the Whisky Run and Pioneer terraces at the Cape Arago and Coquille point sites. Early chronologies for many west coast sites come from Kennedy et al. (1982), who provided leucine D : L ratios for individual sites plotted against isochrons independently constrained by uranium-series ages. These sites were summarized by Simms et al. (2016), who compared tectonically corrected RSL sites to models of Pacific coast glacial isostatic adjustment.

5.1.1 Newport, Oregon

Kelsey et al. (1996) utilized topographic maps and altimeter surveys to map and document the platform elevation ranges of six emergent bedrock terraces which crop out discontinuously through the region due to faulting; we focus on the lowest two of the surveyed platforms, the Newport and Wakonda terraces. Kennedy et al. (1982) first dated the Newport terrace using AAR. The leucine D : L ratio was plotted against isochrons of other AAR ages from proximal locations, assigning the Newport terrace to MIS 5a. Kelsey et al. (1996) assigned terraces to MISs based on soil development stages. Namely, this study assigned the Newport terrace (0–45 m a.p.s.l., above present-day sea level), which is extensive north of Yaquina Bay and discontinuous between Cape Foulweather and Siletz Bay, to MIS 5a; the Wakonda terrace (0–85 m a.p.s.l.) – which is discontinuous from Newport north to Otter Rock and then crops out just above modern beach elevation between Yaquina and Alsea bays before gradually descending below sea level south of Alsea Bay – was assigned to MIS 5c. Based on these age assignments, Kelsey et al. (1996) correlated the Newport and Wakonda terraces to the Whisky Run and Pioneer terraces (see Sect. 5.1.2 Cape Arago). Figures 2 and 3 include the terrace elevations reported by Kelsey et al. (1996), and Figs. 4 and 5 illustrate the MIS assignments for the Newport and Wakonda terraces, respectively (Kennedy et al., 1982; Kelsey et al., 1996).

5.1.2 Cape Arago, Oregon

Griggs (1945) mapped four emergent shore platforms along the central Oregon coastline, of which we focus on the lowest two, the Pioneer and Whisky Run terraces. Adams (1984) documented landward tilting of the Pioneer and Whisky Run terraces and the faults that vertically displace them. No radiometric ages directly constrain the Pioneer and Whisky Run terrace chronology at Cape Arago; instead, these terraces are assigned to MIS 5a and MIS 5c based on correlation to terraces cropping out at Coquille Point (see Sect. 5.1.3 and Figs. 4 and 5). McInelly and Kelsey (1990) published altimeter surveys that revised the peak shoreline angle elevations of the Whisky Run and Pioneer terraces reported by Adams (1984) to 31 and 68 m a.p.s.l., respectively (Figs. 2 and 3). McInelly and Kelsey (1990) also reported the thickness of the sediment packages overlying both terraces and revised the mapped faults that displace each terrace.

5.1.3 Coquille Point, Oregon

This entry focuses on the Pioneer and Whisky Run terraces documented in Griggs (1945). Attribution of the Whisky Run terrace to the MIS 5a substage first appeared in Kennedy et al. (1982) based on leucine D : L ratios on *Saxidomus* and a single uranium-series age on a coral (Fig. 4). Subsequently, 6 uranium-series ages on corals and bryozoans, 10 amino acid ratios on bivalve mollusks *Mya truncata* and *Saxidomus giganteus*, and oxygen isotope stratigraphy on mollusk shells supported the MIS 5a age assignment for the Whisky Run terrace (Kennedy et al., 1982; Muhs et al., 1990, 2006; Fig. 4). McInelly and Kelsey (1990) revisited the region and presented a representative geomorphic cross-section that documented deformation of the Whisky Run terrace by the Pioneer anticline. This survey reported a Whisky Run terrace maximum elevation of 18 m a.p.s.l. (Fig. 2), a small upward revision from the 17 m a.p.s.l. reported by Muhs et al. (1990). No elevation for the Pioneer terrace was reported in the text of this article, though Simms et al. (2016) extracted an elevation of 70 m a.p.s.l. from the cross-section of McInelly and Kelsey (1990). Based on their similar elevations, McInelly and Kelsey (1990) correlated the Pioneer terrace at Coquille Point with the MIS 5c Pioneer terrace at Cape Blanco, itself dated through amino acid ratios and faunal assemblages (Muhs et al., 1990; Fig. 5).

5.1.4 Brookings, Oregon

Kelsey and Bockheim (1994) utilized topographic maps to document seven shore platforms; the lowest two terraces, Harris Butte and Brookings, crop out at bedrock platform elevations of 30–62 and 57–90 m a.p.s.l. (see Figs. 2 and 3), respectively, south of the Whaleshead fault zone. No radiometric ages constrain the age of the Harris Butte and Brookings terraces. These terraces were assigned to MIS 5a and 5c, respectively, based upon similar soil development stages to the Whisky Run and Pioneer terraces at Cape Arago (Figs. 4 and 5).

5.1.5 Bruhel Point, California

Merritts and Bull (1989) surveyed the 14 marine terraces cropping out at Bruhel Point, of which the 10 and 23 m a.p.s.l. terraces (surveyed from the inner edge of the terrace) have been assigned to the MIS 5a and 5c highstands (Figs. 2 and 3). A leucine D : L ratio on the 10 m a.p.s.l. terrace indicates either an MIS 5a or 5c substage designation (Kennedy et al., 1982). In contrast, Merritts and Bull (1989) supported age assignments of MIS 5a and 5c for the 10 and 23 m a.p.s.l. terraces, respectively (see Figs. 4 and 5), based upon correlations made using diagrams of inferred uplift of

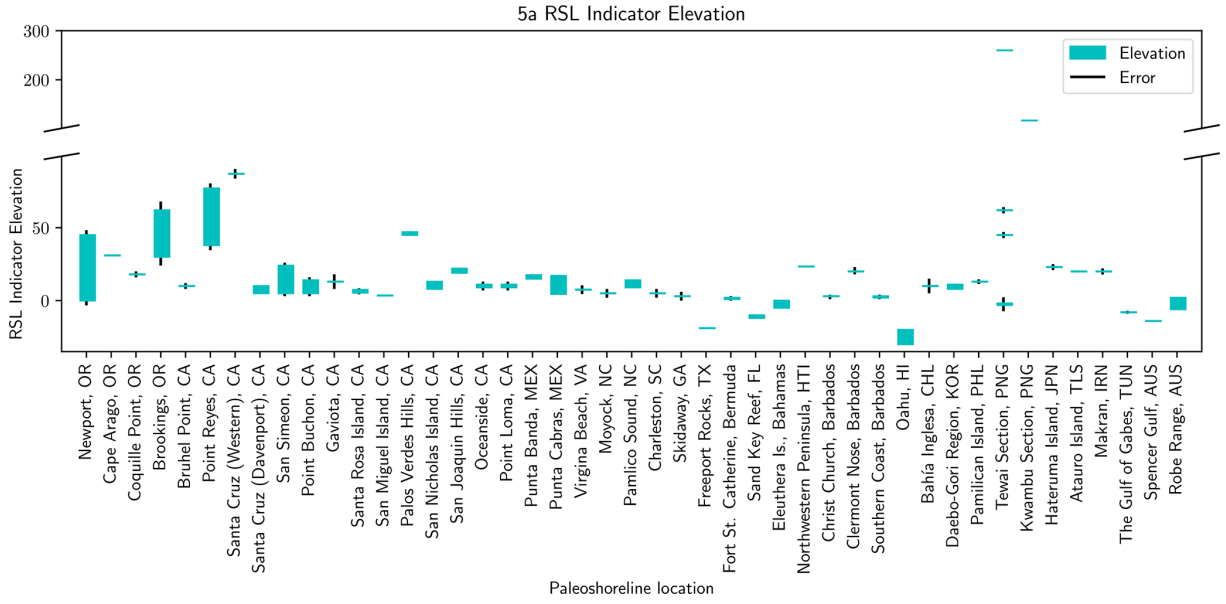

Figure 2. The present elevation of MIS 5a RSL indicators, in meters, at the field locations listed on the horizontal axis. Teal bars represent the full elevation range reported in the primary publications along with the corresponding measurement error, if any, in black bars. Note the scale break on the vertical axis necessary to present indicator elevations for sites with rapid tectonic uplift.

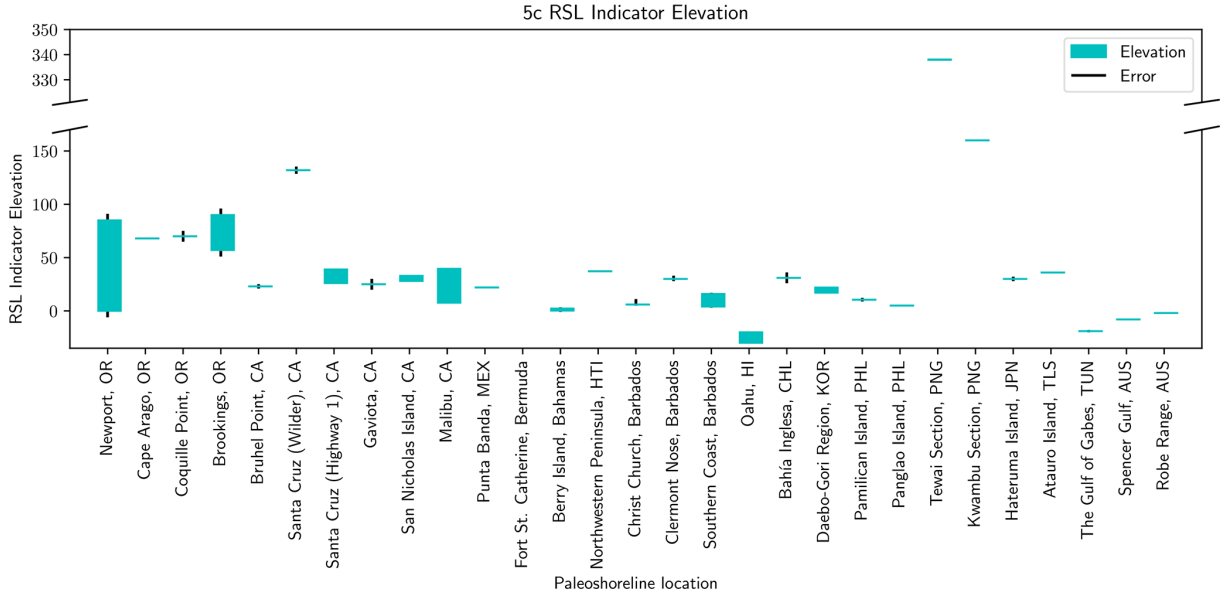

Figure 3. The present elevation of MIS 5c RSL indicators, in meters, at the field locations listed on the horizontal axis. Teal bars represent the full elevation range reported in the primary publications along with the corresponding measurement error, if any, in black bars. Note the scale break on the vertical axis necessary to present indicator elevations for sites with rapid tectonic uplift.

the Bruhel Point terraces vs. inferred ages (uplift-rate diagrams) to the New Guinea sea level curve (see Sect. 5.3.6 Tewai and Kwambu).

5.1.6 Point Reyes, California

Grove et al. (2010) utilized differential GPS to map nine marine terraces across five transects for which the inner edge of the lowest terrace, of purported MIS 5a age, was surveyed between 38–77 m a.p.s.l. (Fig. 2). Five sediment samples overlying the lowest terrace yielded three ages per sample from three energy stimuli: optically stimulated blue-light

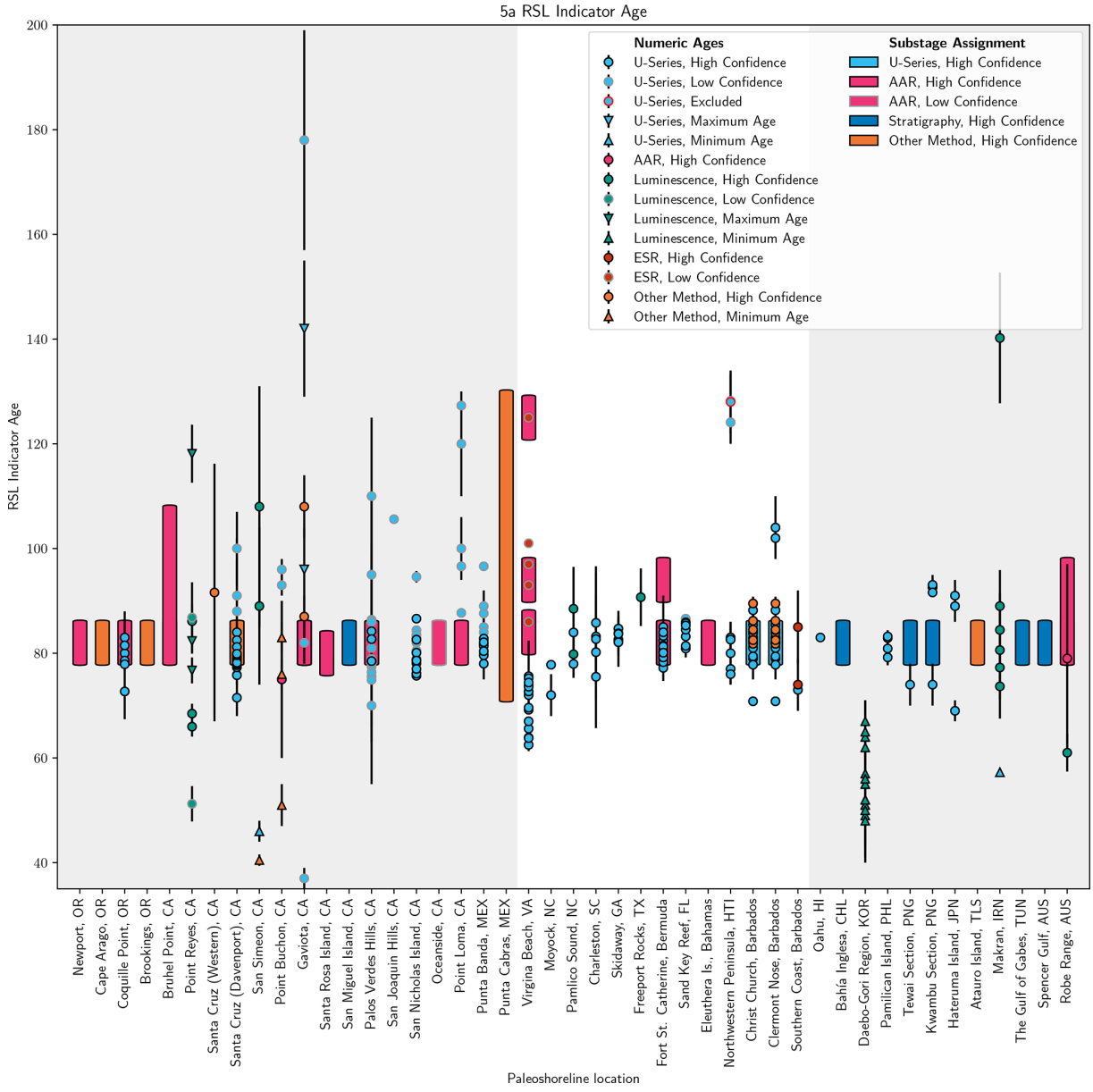

Figure 4. Age assignments for MIS 5a RSL indicators cropping out at the locations listed on the horizontal axis. For each location, the geochronological method is indicated by color; numeric, minimum, and maximum age type by shape; and the confidence of the age by border color. Symbols represent numerical ages, whereas, in the absence of a numeric chronology, bars represent general marine isotope substage assignments (MIS 5c 98–90 ka, MIS 5a 86–72 ka).

luminescence (OSL), optically stimulated infrared luminescence (IRSL), and thermoluminescence (TL). Grove et al. (2010) discounted the OSL ages as being too young (MIS 2–3), whereas these authors interpreted TL ages as maximum ages; the IRSL ages were identified as the most accurate estimates of the time of deposition. The sample identified as the best indicator of terrace age (PR-2) assigns the lowest terrace to MIS 5a; the other four samples yield ages ranging from MIS 3 to MIS 5a or show internal inconsistencies (Fig. 4).

5.1.7 Santa Cruz, California

Alexander (1953) first mapped the emergent marine terraces cropping out in the Santa Cruz, CA, region, for which we focus on (often conflicting) interpretations for the age of the laterally extensive, sediment-mantled terrace formerly named the Santa Cruz terrace as well as the two higher-elevation Western and Wilder terraces later documented by Bradley and Griggs (1976). Bradley and Addicott (1968) presented four uranium-series ages on mollusks that assigned an age to the Santa Cruz terrace – referred to as the "first" terrace

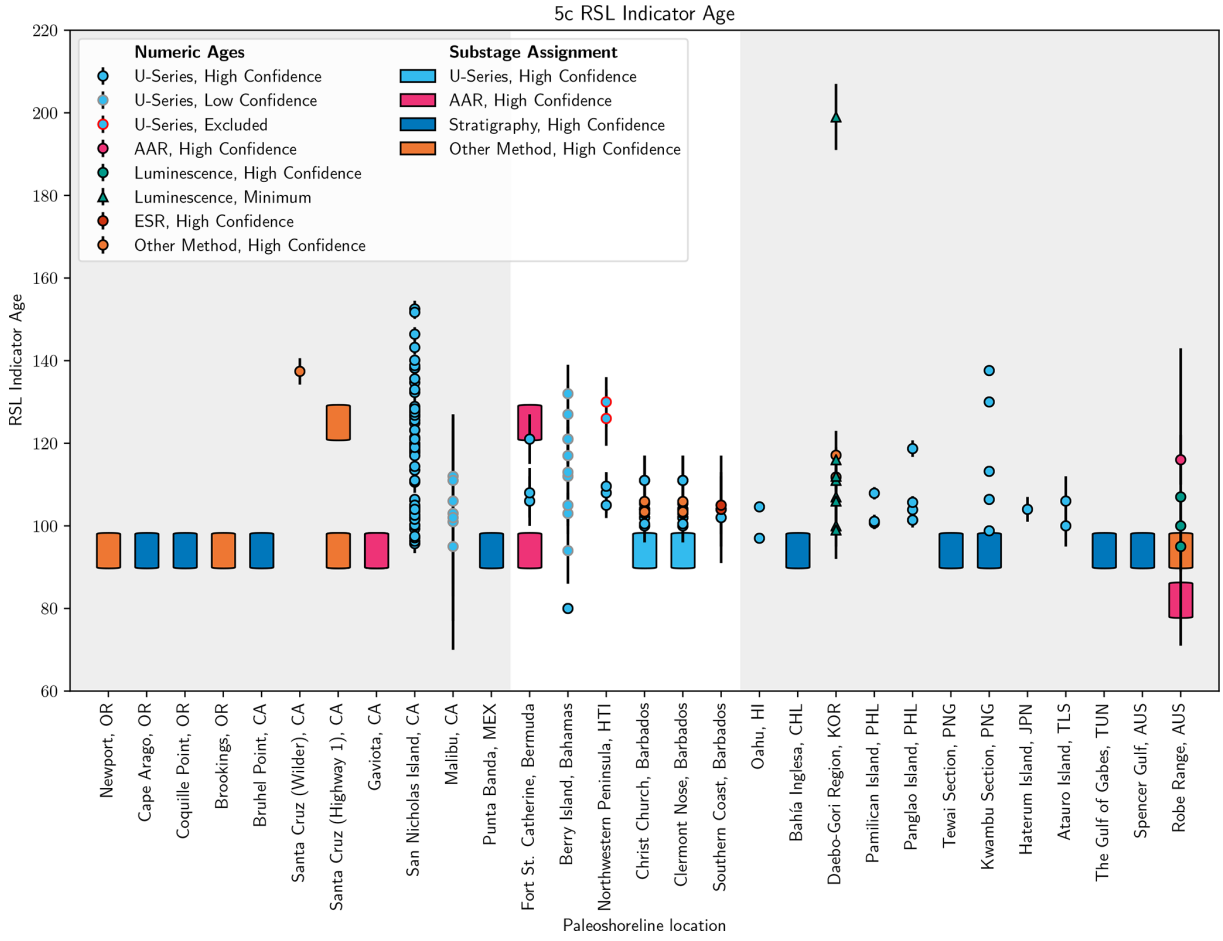

Figure 5. Age assignments for MIS 5c RSL indicators cropping out at the locations listed on the horizontal axis. See Fig. 4 caption for a description of symbols.

in their nomenclature – consistent with either MIS 5a or 5c. Bradley and Griggs (1976) utilized seismic surveys to subdivide the Santa Cruz terrace into three constituent terraces, which, in ascending order of elevation, include the Davenport, Highway 1, and Greyhound terraces. A rich literature discusses the chronostratigraphic assignment of the Davenport and Highway 1 terraces. Most authors have concluded, on the basis of amino acid ratios, diffusion modeling of paleo-sea cliffs, and 15 U-series ages on corals, that the Davenport terrace, which crops out at 5–10 m a.p.s.l. (see Muhs et al., 2006), formed during MIS 5a (Kennedy et al., 1982; Hanks et al., 1984; Muhs et al., 2006). The Highway 1 terrace, at an inner-edge elevation of 26–39 m a.p.s.l. (Bradley and Griggs, 1976), has been alternately assigned to MIS 5c using models of the diffusion of paleo-sea cliffs (Hanks et al., 1984) or to MIS 5e based upon a geologic fault modeling (Valensise and Ward, 1991). In contrast to the above chronology, Perg et al. (2001) presented 10 cosmogenic nuclide ages that assigned the Santa Cruz (undifferentiated), Western (87 m a.p.s.l.; Fig. 2), and Wilder (132 m a.p.s.l.; Fig. 3) terraces to MIS 3, 5a, and 5c, respectively. Muhs et al. (2006) contested these cosmogenic ages, arguing that they date the deposition of alluvium overlying the terraces and therefore provide a minimum age for terrace formation. We report Davenport and Highway 1 as well as Western and Wilder terrace elevations and chronologies as separate entries in the database (see Figs. 2–5) to most accurately represent the existing body of literature. For each terrace all of the reported numeric ages and age assignments are represented, even when conflicting.

5.1.8 San Simeon, California

Hanson et al. (1992) mapped five shore platforms along the San Simeon fault zone. North and south of the fault zone the San Simeon terrace shoreline angle crops out discontinuously between 5–7 and 9–24 m a.p.s.l., respectively (Fig. 2). While a uranium-series age on bone and a radiocarbon age on detrital charcoal provide a minimum terrace age of MIS 3 (Hanson et al., 1992), two thermoluminescence ages on sediment underlying the emergent platform place the San Simeon terrace within the range of MIS 5a to 5c (Berger and Hanson,

1992). Of these possibilities, Simms et al. (2016) elected for the MIS 5a San Simeon terrace age assignment (Fig. 4).

5.1.9 Point Buchon, California

Hanson et al. (1992) mapped a flight of marine terraces across south-central California; the lowest terrace, Q1, with surveyed shoreline angles between 5–14 m a.p.s.l., is overlain by up to 2 m of marine sediment and 15–30 m of non-marine sediment and is cut by several reverse faults (Fig. 2). The Q1 terrace was assigned to MIS 5a based upon three uranium-series minimum ages on marine and terrestrial mammal teeth and bones found in the overlying sediment deposits (Fig. 4). We included in the WALIS database two uranium-series ages on corals considered unreliable by the authors.

5.1.10 Gaviota, California

Rockwell et al. (1992) mapped five well-expressed marine abrasion platforms using transit-stadia surveys; the lowest instance, the Cojo terrace (10–17 m a.p.s.l. shoreline angle; Fig. 2), is found west of the South Branch Santa Ynez fault (SBSYF) and crosses the hinge of the Government Point syncline. Seven uranium-series ages on bone and mollusk (two of which are maximum ages), eight amino acid ratios, and the cool-water aspect of the terrace fauna assign the Cojo terrace to MIS 5a (Rockwell et al., 1992; Kennedy et al., 1992; Fig. 4). Rockwell et al. (1992) correlated the first emergent terrace east of the SBSYF to the Cojo terrace based upon similar amino acid ratios and terrace faunal aspect. While the elevation of the overlying second terrace at this locale was not reported by Rockwell et al. (1992), Simms et al. (2016) extracted an elevation of 25 m a.p.s.l. from an illustration of the shore-parallel terrace profile (see Fig. 2 of Rockwell et al., 1992; Fig. 3). No radiometric ages exist for the second terrace; Rockwell et al. (1992) inferred an MIS 5c age for the second terrace using stratigraphic correlation to the 5a terrace and the cool-water aspect of the terrace fauna (Fig. 5).

5.1.11 California Channel Islands (San Miguel and Santa Rosa islands)

Orr (1968) first mapped marine terraces on northwestern Santa Rosa Island, and later efforts by Dibble and Ehrenspeck (1998) and Pinter et al. (2001) elaborated on both terrace mapping and the geology of the island. Muhs et al. (2014) utilized differential GPS to map the flight of emergent marine terraces on San Miguel and Santa Rosa Island, of which we focus on the lowest terrace at Santa Rosa Island, with a shoreline angle mapped between 5.4–7.4 m a.p.s.l., and the lowest terrace at San Miguel Island, with a shoreline angle mapped at ∼ 3.5 m a.p.s.l. (Fig. 2). Two amino acid ratios on *Chlorostoma* shells assigned the lowest Santa Rosa terrace to MIS 5a (Fig. 4). The lowest San Miguel terrace is overlain by a veneer of fossiliferous cemented gravel and marine sand, which itself is overlain in areas by alluvium (Johnson, 1969; Muhs et al., 2014). Based on stratigraphic position, Muhs et al. (2014) assigned the San Miguel terrace to MIS 5a (Fig. 4).

5.1.12 Palos Verdes Hills, California

Woodring et al. (1946) conducted early mapping of the 13 emergent shore platforms of the Palos Verdes Peninsula; seven early uranium-series ages, each corrected for open-system behavior, assigned the first (lowest) terrace to MIS 5a (Szabo and Rosholt, 1969). Muhs et al. (1992a) showed, on the basis of aminostratigraphy on *Tegula* and *Protothaca* and oxygen isotope data on *Epilucina,* that the "first terrace", as mapped by Woodring et al. (1946), instead represents highstand deposits of both MIS 5a and 5e. Muhs et al. (2006) refined map units and assigned place-based names to supplant the counting scheme of Woodring et al. (1946), redefining the lowest horizontally continuous surface as the Paseo del Mar terrace (the "second" terrace of Woodring et al., 1946) with an estimated shoreline elevation angle of ∼ 45–47 m a.p.s.l. (Fig. 2). A combination of 13 uranium-series ages on *Balanophyllia* and extralimital northern species within the faunal assemblage assigns the Paseo del Mar terrace to MIS 5a (Fig. 4). Around Lunada Bay, Muhs et al. (2006) estimated a ∼ 60–70 m a.p.s.l. elevation shoreline angle for the "third" terrace of Woodring et al. (1946), an unnamed intermediate terrace between the Paseo del Mar (MIS 5a) and Gaffey (MIS 5e; the "fifth" terrace of Woodring et al., 1946); as this terrace does not have geochronological control, we do not include it as an MIS 5c indicator.

5.1.13 San Joaquin Hills, California

Vedder et al. (1957) first mapped the emergent marine terraces at San Joaquin Hills. Grant et al. (1999) extended the mapping of previous unpublished surveys (see the literature discussed therein) and revised the shoreline angle elevation of the first emergent terrace to 19–22 m a.p.s.l. (Fig. 2). Based on a single uranium-series age on coral and correlations between terrace height and presumed eustatic sea level, Grant et al. (1999) argued that either the first terrace formed during MIS 5a and hosts reworked MIS 5c coral or that the MIS 5a and 5c highstands occupied the same terrace (Fig. 4).

5.1.14 San Nicolas Island, California

Vedder and Norris (1963) mapped 14 emergent bedrock-incised marine terraces on San Nicolas Island and documented their associated faunal assemblages. Muhs et al. (1994, 2006) reported 56 uranium-series ages on corals found in multiple outcroppings of the lowermost two terraces (terraces 1 and 2) which assign these to MIS 5a and

5e, respectively (Fig. 4). Muhs et al. (2012) utilized differential GPS measurements to revise previously reported shoreline angle elevations for terraces 1 and 2 and subdivided terrace 2 into two distinct geomorphic units (terraces 2a and 2b). Muhs et al. (2012) argued that, together, the geomorphic relationships and the 65 new uranium-series ages on solitary corals supported the conclusions that (i) terrace 2a (36–38 m a.p.s.l.) formed during MIS 5e; (ii) terrace 2b (28–33 m a.p.s.l.), which hosts corals of ∼ 120 and ∼ 100 ka age clusters, formed during MIS 5c and captures reworked fossils from the adjacent, formerly more extensive 5e terrace (terrace 2a); and (iii) terrace 1 (8–13 m a.p.s.l.) formed during MIS 5a. Muhs et al. (2012) argued that the distinctive faunal assemblages of terraces 1, 2a, and 2b serve to further support their different ages. The terrace elevations reported by Muhs et al. (2012) are shown in Figs. 2 and 3; Figs. 4 and 5 show the full suite of uranium-series ages reported for San Nicolas Island terraces 1, 2a, and 2b (Muhs et al., 1994; 2006; 2012). The MIS 5a and 5c WALIS entries include uranium-series ages MH12-001-001–MH12-055-001 and MH12-057-001 from Chutcharavan and Dutton (2021).

5.1.15 Point Loma and Oceanside, California

Ellis (1919) first mapped five marine terraces at Point Loma. Hertlein and Grant (1944) briefly revisited the lower terraces. Carter (1957) extended the mapping to include an additional terrace cropping out lower than the lowest terrace surveyed by Ellis (1919), later named Bird Rock terrace (Kern, 1977). Kern (1973) documented deformation of the Point Loma terraces. Kern and Rockwell (1992) utilized hand levels to revise the shoreline angle elevation of the Bird Rock terrace to 9–11 m a.p.s.l. (Fig. 2). The outcropping of Bird Rock terrace to the west at Oceanside is also mapped at 9–11 m a.p.s.l. (Fig. 2). Ku and Kern (1974) reported two uranium-series ages on mollusks but did not utilize these to assign an age to Bird Rock terrace due to secondary uptake of uranium in the mollusk shells. Uranium-series ages MH02-056-001 derive from Chutchavaran and Dutton (2021). In the absence of radiometric ages, calibrated amino acid ratios support a Bird Rock terrace age assignment to MIS 5a (Kern, 1977; Kern and Rockwell, 1992; Fig. 4).

5.1.16 Malibu, California

Davis (1932) mapped three emergent marine terraces around Malibu, California, which, in ascending order, are named the Monic, Dume, and Malibu terraces, of which we focus on the westward-tilting Dume terrace. Birkeland (1972) revisited the Dume terrace, of which the shoreline angle sits between ∼ 7 and 40 m a.p.s.l. (Fig. 3). Szabo and Rosholt (1969) reported seven uranium-series ages on mollusks sampled from the Dume terrace consistent with an MIS 5c age (Fig. 5), though these ages utilized an open-system model to compensate for mobile uranium within shells. If correct, these radiometric ages imply that the Dume terrace correlates with San Nicolas Island terrace 2 (Birkeland, 1972; see above). Szabo and Rosholt (1969) and Birkeland (1972) documented a higher adjacent terrace, referred to as "terrace C" or "Corral terrace", which crops out between the Malibu and Dume terraces. Szabo and Rosholt (1969) utilized the same corrected uranium-series methods to assign the Corral terrace to MIS 5e.

5.1.17 Punta Banda, Mexico

Lindgren (1889) first documented Punta Banda marine terraces, and Allen et al. (1960) and Rockwell et al. (1989) mapped the lowest 13 and 12 terraces in detail, respectively. The Lighthouse terrace, the lowest mapped terrace (15–17.5 m a.p.s.l. shoreline angle; Fig. 2), is well preserved on the south side of the peninsula, though discontinuous on the north side (Rockwell et al., 1989). Fifteen uranium-series ages on *Balanophyllia elegans* assign the Lighthouse terrace to MIS 5a, and extralimital northern species in the faunal assemblage support this designation (Rockwell et al., 1989; Fig. 4). A fragmented, narrow second terrace crops out across the Punta Banda peninsula with a shoreline angle of 22 m a.p.s.l. (Rockwell et al., 1989; Fig. 3). No radiometric ages exist for the second terrace, though stratigraphic relationships imply an age of MIS 5c (see discussion in Rockwell et al., 1989; Fig. 5).

5.1.18 Punta Cabras, Mexico

At Punta Cabras, Baja California, Mexico, Addicott and Emerson (1959) first documented a narrow, discontinuous marine terrace with inner-edge elevations of 4.5–17 m a.p.s.l. (Fig. 2). No radiometric ages exist for this terrace, though a limited number of radiocarbon ages and extralimital northern species in the faunal assemblage of overlying marine and non-marine deposits support a terrace assignment to MIS 5a (Addicott and Emerson, 1959; Mueller et al., 2009; Fig. 4).

5.1.19 Summary

Marine terraces comprise the entirety of MIS 5a and 5c relative sea level indicators cropping out along the North American Pacific coast. While in principle marine terraces can serve as excellent quality indicators (see 3 and 4), Pacific coast marine terraces receive quality ratings from very poor (1) to average (3) (Fig. 6a and d and Tables 1 and 2). These ratings reflect four systematic uncertainties. First, no primary reference reports a terrace's indicative range, the distance between the storm wave swash height and the wave breaking depth (Vacchi et al., 2014; Rovere et al., 2016), and this precludes a calculation of indicative meaning. Given this absence, we used the IMCalc software to quantify the indicative meaning of all Pacific coast marine terraces (WALIS RSL IDs 3473–3503; Lorscheid and Rovere, 2019). The arising

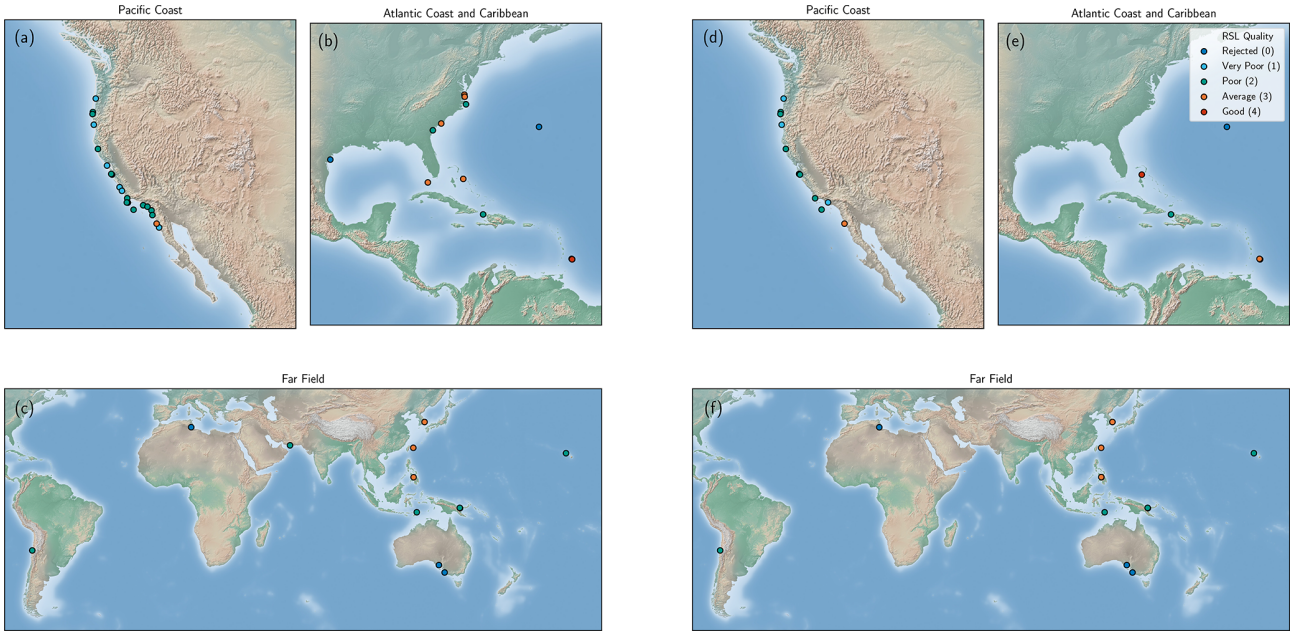

Figure 6. MIS 5a **(a–c)** and MIS 5c **(d–f)** sea level indicator elevation quality ratings atop the Matplotlib Basemap Shaded Relief map (Hunter, 2007). For the five Iranian subsites we plotted the lowest quality ratings of those listed in Tables 1 and 2.

indicative ranges tend to vary between 4 and 7.5 m, which necessitates quality ratings of poor (2) and lower (as for MIS 5a and 5c terraces at Cape Arago, Coquille Point, Bruhel Point, Gaviota, and San Nicolas Island; MIS 5a terraces at Santa Cruz (Western and Davenport), San Miguel Island, Santa Rosa Island, Oceanside, and Point Loma; and the MIS 5c terrace at Santa Cruz, and Wilder). The MIS 5a and 5c terraces at Punta Banda are the sole exception as these elevation measurements are sufficiently precise to warrant average quality (3) ratings. Second, the primary literature rarely reports the reference datum for the RSL indicator elevation. Third, the use of altimetry and topographic map measurement techniques before the widespread adoption of differential GPS means that literature-reported measurement uncertainties generally exceed ~ 3 m (as for the MIS 5a terraces at Palos Verdes Hills and San Joaquin Hills). Fourth, many regional terraces also crop out over a range of elevations due to faulting or tilting, and this range further contributes to RSL uncertainty (such as for MIS 5a and 5c terraces at Newport and Brookings; MIS 5a terraces at Point Reyes, San Simeon, Point Buchon, and Punta Cabras; and MIS 5c terraces at Santa Cruz (Highway 1) and Malibu). As all four systematic uncertainties apply to many Pacific coast marine terraces, and at least one uncertainty applies to all terraces, the Pacific coast yields quality ratings of very poor (1) to average (3). From this we conclude that revisiting indicator elevation measurements with modern mapping methods could better constrain Pacific coast MIS 5a and 5c terrace elevations, indicative meanings, and RSL uncertainties.

We assigned the chronologies of the North American Pacific coast marine terrace ratings from good (4) to poor (2) (Fig. 7a and d and Tables 1 and 2). The three methods that conferred good quality (4) ratings for this region include first, reproducible, high-precision uranium-series ages on solitary coral skeletal carbonate (as for MIS 5a terraces at Coquille Point, Santa Cruz (Davenport terrace), Palos Verdes Hills, San Nicholas Island, and Punta Banda); second, high-precision luminescence ages (as for the MIS 5a Point Reyes marine terrace); and third, AAR on mollusks (the MIS 5a and 5c terraces at Gaviota and the MIS 5a terraces at Newport, Santa Rosa Island, and Oceanside). For chronologic methods that yielded age uncertainty beyond the bounds of an MIS 5 substage – often arising from substrate experiencing open-system diagenesis – we applied an average (3) quality rating. Examples of this include uranium-series ages on coral (the MIS 5a terrace at San Joaquin Hills and the MIS 5c terrace at Malibu) or mollusks (the MIS 5a terrace at Point Loma), cosmogenic ages (the MIS 5a and 5c terraces at Santa Cruz, Western, and Wilder), radiocarbon ages (the MIS 5a terrace at Punta Cabras), luminescence ages (the MIS 5a terrace at San Simeon), and AAR on mollusks (the MIS 5a terrace at Bruhel Point). While Muhs et al. (2012) interpreted the MIS 5c and 5e uranium-series ages on corals from San Nicholas Island Terrace 2b as an indication of terrace reoccupation, which could afford a good (4) quality rating, here we assign Terrace 2b an average (3) quality rating given that these ages span a time interval longer than either individual MIS. Poor quality (2) chronology ratings arise from the relative dating method of terrace counting (MIS 5a and 5c terraces

Table 1. The location name, latitude and longitude, elevation, indicator type, dating method, and assigned elevation and age quality ratings for marine isotope stage 5a indicators.

Site	Latitude	Longitude	Elevation	Indicator type[a]	Dating method	Indicator quality	Age quality
Newport	44.63	−124.05	(0–45) ± 3.3	SLI	AAR, other	1	4
Cape Arago	43.306531	−124.401657	31 ± 2	SLI	Other	2	2
Coquille Point	43.114117	−124.437096	18 ± 2	SLI	U-series, AAR	2	4
Brookings	42.05	−124.28	(30–62) ± 6	SLI	Other	1	2
Bruhel Point	39.607469	−123.786856	10 ± 2	SLI	Stratigraphy, AAR	2	3
Point Reyes	37.9	−122.6938	(38–77) ± 3.4	SLI	Luminescence	1	4
Santa Cruz (Western terrace)	36.96	−122.09	87 ± 3.3	SLI	Other	2	3
Santa Cruz (Davenport terrace)	37.0294755	−122.1923133	(5–10)	SLI	U-series, AAR, other	2	4
San Simeon[b]	35.639462	−121.1848936	(5–24) ± 2	SLI	U-series, luminescence, other	1	3
Point Buchon	35.2552529	−120.8990702	(5–14) ± 2	SLI	U-series, other	1	2
Gaviota	34.4675398	−120.2674989	(10–17) ± 2	SLI	U-series, AAR, other	2	4
Santa Rosa Island	34.003812	−120.195602	(5.4–7.4) ± 1	SLI	AAR	2	4
San Miguel Island	34.0191768	−120.3177209	3.5	SLI	Stratigraphy	2	2
Palos Verdes Hills	33.7246996	−118.3552086	(45–47)	SLI	U-series, AAR	2	4
San Joaquin Hills	33.5696784	−117.8385408	(19–22)	SLI	U-series	2	3
San Nicolas Island	33.2472453	−119.5070695	(8–13) ± 0.3	SLI	U-series	2	4
Oceanside	33.17	−117.35	(9–11) ± 2	SLI	AAR	2	4
Point Loma	32.67	−117.24	(9–11) ± 2	SLI	U-series, AAR	2	3
Punta Banda	31.7455541	−116.7394247	(15–17.5) ± 0.2	SLI	U-series	3	4
Punta Cabras	31.33	−116.44	(4.5–17)	SLI	Other	1	3
Virginia Beach	36.7823	−76.1966	7.5 ± 3	SLI	U-series, AAR, ESR	3	4
Moyock	36.508	−76.153	5 ± 3	SLI	U-series	3	4
Pamlico Sound	35.4828287	−75.951469	(9–14)	SLI	Luminescence	2	4
Charleston	32.8586	−79.7803	5 ± 3	SLI	U-series	3	4
Skidaway	31.916	−81.071	3 ± 3	SLI	U-series	2	4
Freeport Rocks	27.7852552	−96.9132876	−18.9	TL	Luminescence	0	4
Fort St. Catherine	32.390733	−64.674732	(1–2) ± 1	TL	U-series, AAR	0	4
Sand Key Reef	24.4977811	−81.8477838	(−12 to −10)	SLI	U-series	3	4
Eleuthera Island	25.0090818	−76.3780482	(−5–0)	SLI	AAR	3	4
Northwestern Peninsula	19.8039797	−73.3097345	23.4	SLI	U-series	2	4
Christ Church	13.0699141	−59.5693843	3 +1/−2	SLI	U-series, other	4	4
Clermont Nose	13.1350465	−59.6345479	20 +3/−2	SLI	U-series, other	3	3
Southern coast	13.0698341	−59.5409821	(2–3) ± 1	SLI	U-series, ESR	3	4
Oahu	21.4477881	−158.1997812	(−30 to −20)	SLI	U-series	2	4
Bahía Inglesa	−27.1142508	−70.8742622	10 ± 5	SLI	Stratigraphy	2	2
Daebo–Gori region	36.0554812	129.5444388	(8–11)	SLI	Luminescence	3	2
Pamilacan Island	9.4951118	123.9281264	6 ± 1	SLI	U-series	3	4
Tewai section	−6.2206748	147.6766172	260	SLI	U-series, stratigraphy	2	4
Kwambu section	−6.0704502	147.5171788	117	SLI	U-series, stratigraphy	2	3
Hateruma Island	24.058648	123.7817205	23 ± 2	SLI	U-series	3	3
Atauro Island	−8.3012532	125.5565624	20	SLI	Other	2	2
Lipar	25.2567922	60.80393	20 ± 2.1	SLI	U-series, luminescence	3	4
Lipar	25.2591769	60.7979098	45 ± 2.1	SLI	Luminescence	3	4
Ramin	25.2694195	60.763467	−2 ± 4.3	SLI	Luminescence	2	3
Gurdim	25.3390736	60.1665682	62 ± 2.1	SLI	Luminescence	3	4
Jask	25.6552358	57.7874395	−3 ± 4.3	SLI	Luminescence	2	4
Bsissi	33.7171283	10.313814	−8 ± 1	TL	Stratigraphy	0	2
Ghannouche	33.7072534	10.3343664	−9 ± 1	TL	Stratigraphy	0	2
Teboulbou	33.7007635	10.3519874	−8 ± 1	TL	Stratigraphy	0	2
Kettana	33.6785967	10.4125647	−9 ± 1	TL	Stratigraphy	0	2
Zarat	33.6785967	10.4125647	−8 ± 1	TL	Stratigraphy	0	2
Spencer Gulf	−33.9120079	136.8615574	−8	ML	Other	0	2
Robe Range	−37.219789	139.787838	(−6–2)	TL	AAR, other	0	3

[a] SLI: sea level indicator; TL: terrestrial-limiting; ML: marine-limiting. [b] Terrace chronology does not differentiate MIS 5 substage.

at Bruhel Point; the MIS 5a terrace at San Miguel Island; and the MIS 5c terraces at Cape Arago, Coquille Point, and Punta Banda). For this region, chronologic assignment by terrace counting is especially common for MIS 5c terraces with an adjacent, well-dated MIS 5a terrace. Non-traditional methods and maximum and minimum limiting ages confer a poor (2) rating for MIS 5a and 5c terraces at Newport, Brookings, and Gaviota; the MIS 5a terrace at Cape Arago; and the MIS 5c terrace at Santa Cruz (Highway 1 terrace). Likewise, minimum limiting uranium-series age on mammal

Table 2. Marine isotope stage 5c.

Site	Latitude	Longitude	Elevation	Indicator type[a]	Dating method	Indicator quality	Age quality
Newport	44.63	−124.05	(0–85) ± 6	SLI	Other	1	2
Cape Arago	43.306531	−124.401657	68 ± 2	SLI	Stratigraphy	2	2
Coquille Point	43.114117	−124.437096	70 ± 2	SLI	Stratigraphy	2	2
Brookings	42.05	−124.28	(57–90) ± 6	SLI	Other	1	2
Bruhel Point	39.607469	−123.786856	23 ± 2	SLI	Stratigraphy	2	2
Santa Cruz (Wilder terrace)	36.96	−122.09	132 ± 3.3	SLI	Other	2	3
Santa Cruz (Highway 1 terrace)	37.0294755	−122.1923133	26	SLI	Other	1	2
Gaviota	34.4675398	−120.2674989	25 ± 5	SLI	AAR, other	2	4
San Nicolas Island	33.2472453	−119.5070695	(28–33) ± 0.3	SLI	U-series	2	3
Malibu	34.03	−118.71	(7.6–39.6)	SLI	U-series	1	3
Punta Banda	31.7455541	−116.7394247	22 ± 0.2	SLI	Stratigraphy	3	2
Fort St. Catherine	32.390733	−64.674732	Not Reported	TL	U-series, AAR	0	3
Berry Islands	25.6250042	−77.8252203	(0.2–2.3) ± 1	SLI	U-series	4	3
Northwestern Peninsula	19.8039797	−73.3097345	37.2	SLI	U-series	2	4
Christ Church	13.0699141	−59.5693843	6 +5/ − 1	SLI	U-series, other	2	4
Clermont Nose	13.1350465	−59.6345479	30 +3/−2	SLI	U-series, other	3	4
Southern coast	13.0698341	−59.5409821	(4–16) ± 1	SLI	U-series, ESR	2	4
Oahu	21.4477881	−158.1997812	(−30 to −20)	SLI	U-series	2	4
Bahía Inglesa	−27.1142508	−70.8742622	31 ± 5	SLI	Stratigraphy	2	2
Daebo–Gori region	36.0554812	129.5444388	(17–22)	SLI	Luminescence, other	3	2
Pamilacan Island	9.4951118	123.9281264	13 ± 1.6	SLI	U-series	3	4
Panglao Island	9.573798	123.8221394	5	SLI	U-series	3	4
Tewai section	−6.2206748	147.6766172	338	SLI	Stratigraphy	2	2
Kwambu section	−6.0704502	147.5171788	160	SLI	U-series, stratigraphy	2	3
Hateruma Island	24.058648	123.7817205	30 ± 2	SLI	U-series	3	4
Atauro Island	−8.3012532	125.5565624	36	SLI	U-series	2	4
Zarat	33.6785967	10.4125647	−18 ± 1	TL	Stratigraphy	0	2
Zerkine	33.6785967	10.4125647	−18 ± 1	TL	Stratigraphy	0	2
Zerkine	33.6785967	10.4125647	−20 ± 1	TL	Stratigraphy	0	2
Spencer Gulf	−33.9120079	136.8615574	−14	ML	Other	0	2
Robe Range	−37.219789	139.787838	−2	TL	AAR, luminescence, other	0	4

[a] SLI: sea level indicator; TL: terrestrial-limiting; ML: marine-limiting.

teeth and bone and unreliable uranium-series dates on coral (see Hanson et al., 1992) assign Point Buchon a poor quality rating (2). For the North American Pacific coast, MIS 5a terraces generally received higher quality ratings than MIS 5c terraces (Tables 1 and 2).

5.2 North American Atlantic coast and the Caribbean

5.2.1 Virginia Beach, Virginia; Moyock, North Carolina; Charleston, South Carolina; and Skidaway, Georgia

Cronin et al. (1981) mapped emergent coral terraces along the Atlantic coast of the United States, from Virginia to Georgia, and reported reconstructions of paleo-sea level based upon their documented terrace elevations. Wehmiller et al. (2004) revisited the Virginia Beach, Moyock, Charleston, and Skidaway sites and reported the maximum elevation of the four coral-bearing units as ∼7.5, ∼5, ∼5, and ∼3 m a.p.s.l., respectively (Fig. 2). A total of 27 uranium-series ages on corals assign the terraces at these 4 sites to MIS 5a (Cronin et al., 1981; Szabo, 1985; Wehmiller et al., 2004; see Fig. 4). Further, five electron spin resonance ages and eight amino acid ratios at the Virginia Beach site support an age assignment of MIS 5 sensu lato, without a specific substage designation (Mirecki et al., 1995). No MIS 5c-equivalent coral terraces were recognized across this region.

5.2.2 Pamlico Sound, North Carolina

Parham et al. (2013) utilized outcrops and sediment cores to map late Quaternary beach deposits, of which we focus on a deposit primarily composed of a thin veneer of sand and laminated sand. The sequence appears discontinuously through the study site at an elevation of 9–14 m a.p.s.l. (Fig. 2): east of the Chowan River, the deposit forms a prograding spit, whereas further east of the Suffolk shoreline the deposit forms a seaward-thickening wedge, and the deposit is not well preserved in the northern and southern portions of the study area. Shelly marine material within the deposit was assigned to MIS 5a using calibrated amino acid racemization and optically stimulated luminescence dating (Fig. 4). Two uranium-series ages now support an MIS 5a age assignment for these beach deposits (Wehmiller et al., 2021a). See Wehmiller (2021b) for a comprehensive database of AAR ages for the North American Atlantic coast.

5.2.3 Freeport Rocks, Texas

Simms et al. (2009) documented a sedimentary deposit within offshore sediment cores, referred to as the Freeport Rocks Bathymetric High, consisting of barrier island facies. The deposit appears at its highest elevation within the core at 18.9 m b.p.s.l. (below present-day sea level; Fig. 2). The authors assign the Freeport Rocks Bathymetric High to MIS 5a based upon a single optically stimulated luminescence age (Fig. 4).

5.2.4 Fort St. Catherine, Bermuda

A rich literature describes the evolution of the stratigraphic nomenclature of Bermuda, comprised of six carbonate units separated by *terra rosa* paleosols (Land et al., 1967; Vacher and Hearty, 1989; Hearty, 2002). The marine member of the Southampton Formation, mapped at 1 m a.p.s.l. (Vacher and Hearty, 1989), was tentatively assigned to MIS 5a or 5c using amino acid stratigraphy (Harmon et al., 1983; Hearty et al., 1992), though, subsequently, 24 uranium-series ages reported across multiple studies have indicated an MIS 5a age assignment (Harmon et al., 1983; Ludwig et al., 1996; Muhs et al., 2002; see Fig. 4). The Pembroke unit of the Rocky Bay Formation, previously classified as the Pembroke Formation (with a proposed alternate name of the Hungry Bay Formation), has generated more debate. Amino acid ratios on *Poecilozonites* support a MIS 5c age assignment (Harmon et al., 1983), while whole-rock amino acid ratios support an age assignment of MIS 5e (Hearty et al., 1992). Four uranium-series ages yielded one MIS 5e coral, two MIS 5c-aged corals, and one modern coral (Harmon et al., 1983; see Fig. 5), though Vacher and Hearty (1989) argued that published uranium-series ages were unable to resolve an MIS 5 substage for the Rocky Bay Formation and instead hypothesized that this unit represents MIS 5e. For the purposes of this review, the Pembroke unit chronology is included in Fig. 5, with both 5c and 5e age assignments included. No elevation was reported for the Pembroke unit.

Moreover, controversy exists over the classification of both the Southampton Formation and the Pembroke unit of the Rocky Bay Formation. Harmon et al. (1983) hypothesized that both units formed from storm wave activity, and, thus, the deposits do not serve as indicators of a sea level highstand. Toscano and Lundberg (1999) supported this hypothesis, further specifying that the units were formed in the Holocene and incorporated corals of many different ages. Alternatively, other studies argued the location of Fort St. Catherine relative to the platform margin, and the narrow range of MIS 5a ages on corals found within the Southampton Formation reveal that these units represent a sea level highstand (Vacher and Hearty, 1989; Ludwig et al., 1996; Muhs et al., 2002). Here we include both units within the database.

5.2.5 Sand Key Reef, Florida

Seismic-reflection profiles documented submerged outlier reefs along the windward side of the modern Florida Keys (Lidz et al., 1991; Ludwig et al., 1996; Toscano and Lundberg, 1999). While the Sand Key Reef shows geomorphic complexity, the primary reef crest sits ∼10–12 m b.p.s.l. (Fig. 2). The reef primarily comprises *Montastrea annularis*, with a thin overgrowth of reef crest *Acropora palmata* (Ludwig et al., 1996). Two radiocarbon ages along with eight uranium-series ages on *Montastrea annularis*, *Acropora palmata*, and *Colpophyllia natans* assign the main reef growth to MIS 5a (Lidz et al., 1991; Ludwig et al., 1996; Toscano and Lundberg, 1999; Fig. 4).

5.2.6 Eleuthera Island, Bahamas

Skeletal eolianites comprising Eleuthera Island are interpreted as eolian dunes and are separated from the underlying formations by paleosols (Kindler and Hearty, 1996; Hearty, 1998; Hearty and Kaufman, 2000). The authors report an inferred paleo-sea level of 0–5 m b.p.s.l. rather than the modern elevation of the deposit (Hearty and Kaufman, 2000; Fig. 2). The stratigraphic position, location, and amount of diagenetic alteration of the eolianite, along with whole-rock amino acid ratios, assign the unit to MIS 5a (Fig. 4).

5.2.7 Berry Islands, Bahamas

Newell (1965) reported a single uranium-series age for a coral welded with caliche to a platform on the Berry Islands, which assigned the coral to MIS 5a. Neumann and Moore (1975) reported 11 additional uranium-series ages on corals found at 0.2–2.3 m a.p.s.l. (Fig. 3) as MIS 5 in age, though the range of ages could not assign the ridge to a specific substage highstand. Creveling et al. (2017) noted that an MIS 5c age assignment for the Berry Islands corals fits the published age uncertainty (Fig. 5).

5.2.8 Northwestern Peninsula, Haiti

Woodring et al. (1924) first documented the geology of the Northwestern Peninsula, which was followed by further research summarized by Dodge et al. (1983). Dodge et al. (1983) mapped seven constructional coral reef terraces composed primarily of *Acropora palmata*, of which we focus on the lowest two, the Mole and Saint terraces. Dumas et al. (2006) published altimeter surveys for the Mole and Saint terraces (also referred to as T1 and T2), revising the previously reported inner-edge elevations to 23 and 37 m a.p.s.l., respectively (Figs. 2 and 3). Dodge et al. (1983) and Dumas et al. (2006) argued that 15 uranium-series ages on corals support the conclusion that (i) the Mole terrace formed during MIS 5a; (ii) the Saint terrace formed during MIS 5c; and (iii) both terraces host corals reworked from the adjacent MIS 5e terrace (see Figs. 4 and 5).

5.2.9 Christ Church and Clermont Nose traverses, southern coast of Barbados

Mesolella (1967) first mapped the coral reef terraces of the Christ Church and Clermont Nose traverses. Bender et al. (1979) revisited nine reef tracts at Christ Church and seven reef tracts at Clermont Nose. A total of 28 uranium-series ages on corals, along with 12 protactinium-231 ages, assign the Worthing and Ventor terraces at both traverses to MIS 5a and 5c, respectively (Broecker et al., 1968; Mesolella, 1969; Bender et al., 1979; Bard et al., 1990; Edwards et al., 1997; see Figs. 4 and 5). The elevations of the Worthing and Ventor terraces are mapped at 3 and 6 m a.p.s.l. at Christ Church and 20 and 30 m a.p.s.l. at Clermont Nose (Figs. 2 and 3). Schellmann and Radtke (2004) mapped additional terraces on the southern coast. The two sub-terraces T-1a_1 and T-1a_2 were collectively mapped at 2–3 m a.p.s.l. and assigned to MIS 5a based on two averaged ESR ages and one uranium-series age (Figs. 2 and 4). The sub-terraces T-1b, T-2, and T-3 were collectively mapped at 4–16 m a.p.s.l. and assigned to MIS 5c based on three averaged ESR ages and one uranium-series age (Figs. 3 and 5).

5.2.10 Summary

The North American Atlantic coast and Caribbean sea level indicators, which consist of coral reef terraces, beach deposits, and terrestrial-limiting beach ridges, received elevation quality ratings from good (4) to rejected (0) (Fig. 6b and e and Tables 1 and 2). Since none of the primary literature sources report indicative ranges for the relative sea level indicators along the North Atlantic coast and Caribbean, we calculated these values with the IMCalc software and reported these for WALIS RSL IDs 3504–3508, 3511–3519, 3556, and 3983–3984 (Lorscheid and Rovere, 2019). The clear reference datum for the Berry Islands and MIS 5a Christ Church coral reef terraces (Neumann and Moore, 1975; Bender et al., 1979) warrants the only good quality (4) ratings for this region. For MIS 5a and 5c Clermont Nose and those coral reef terraces with no reference data reported (as for MIS 5a RSL indicators at Virginia Beach, Moyock, Charleston, Sand Key Reef, Eleuthera Island, and southern coast of Barbados), the assigned quality ratings of average (3) reflect the precision of the elevation measurement reported in the primary literature and indicative ranges equal to or less than $\sim$ 2 m as calculated by IMCalc. Coral reef terraces and beach deposits with a poor quality rating (2) reflect either a greater elevation measurement uncertainty (as for the MIS 5a and 5c RSL indicators at Northwestern Peninsula; the MIS 5a indicator at Pamlico Sound; and the MIS 5c indicators at Christ Church and southern coast of Barbados) or an indicative range greater than $\sim$ 2 as calculated by IMCalc (as for MIS 5a Skidaway). The terrestrial-limiting MIS 5a indicator at Freeport Rocks and the MIS 5a and 5c indicators at Fort St. Catherine warrant a rejected (0) quality rating. As with the Pacific coast indicators, we support revisiting coral reef terraces and beach deposits with quality ratings of average (3) to poor (2) to improve uncertainty by applying modern methods for elevation measurement and adopting an updated framework to constrain indicative meaning.

We assigned the North American Atlantic coast and Caribbean chronologies ratings of good (4) to average (3) (Fig. 7b and e and Tables 1 and 2). For this region, good ratings (4) arose from one of three methods: first, high-precision uranium-series ages from skeletal coral (from MIS 5a and 5c indicators at Northwestern Peninsula, Christ Church, and southern coast; MIS 5a indicators at Virginia Beach, Moyock, Charleston, Skidaway, Sand Key Reef, and Fort St. Catherine; and the MIS 5c indicator at Clermont Nose); second, high-precision luminescence ages (on MIS 5a indicators at Pamlico Sound and Freeport Rocks); and third, AAR dating (at Eleuthera Island). Sites that receive an average quality rating (3) have uranium-series-based chronologies which span MIS 5 (the MIS 5a indicator at Clermont Nose and the MIS 5c indicators at Fort St. Catherine and the Berry Islands). We advocate continued focus on sites with average quality ratings (3) – those that have substrate amenable to geochronology yet have imprecise ages – to improve chronologic assignments.

5.3 Far field

5.3.1 Oahu, Hawaii

Sherman et al. (2014) utilized offshore drill cores to document and date two submerged coral reef terraces on Oahu. A single uranium-series age assigned one terrace to MIS 5a; two uranium-series ages assigned a second terrace to MIS 5c (Figs. 4 and 5), though distinct elevations were not reported for the MIS 5a and 5c terraces. Instead, a range of elevations from 20–30 m b.p.s.l. were provided for both terraces (Figs. 2 and 3).

5.3.2 Bahía Inglesa, Chile

Marquardt et al. (2004) utilized altimeter surveys to map eight emergent marine terraces and the overlying fossiliferous terrace deposits. The shoreline angle of the two lowest terraces found above the Holocene beach is mapped at 10 and 31 m a.p.s.l. (Figs. 2 and 3). Uranium-series and electron spin resonance ages from a neighboring region assign the two terraces to MIS 5, and their stratigraphic position, assuming uniform uplift rate, further assigns the 10 and 31 m terraces to MIS 5a and 5c (see discussion in Marquardt et al., 2004; Figs. 4 and 5).

5.3.3 Daebo–Gori region, Korea

Choi et al. (2008) utilized differential GPS to map marine platforms in the Daebo–Gori region. The T2 terrace, with a shoreline angle mapped at 8–11 m a.p.s.l. (Fig. 2), is a

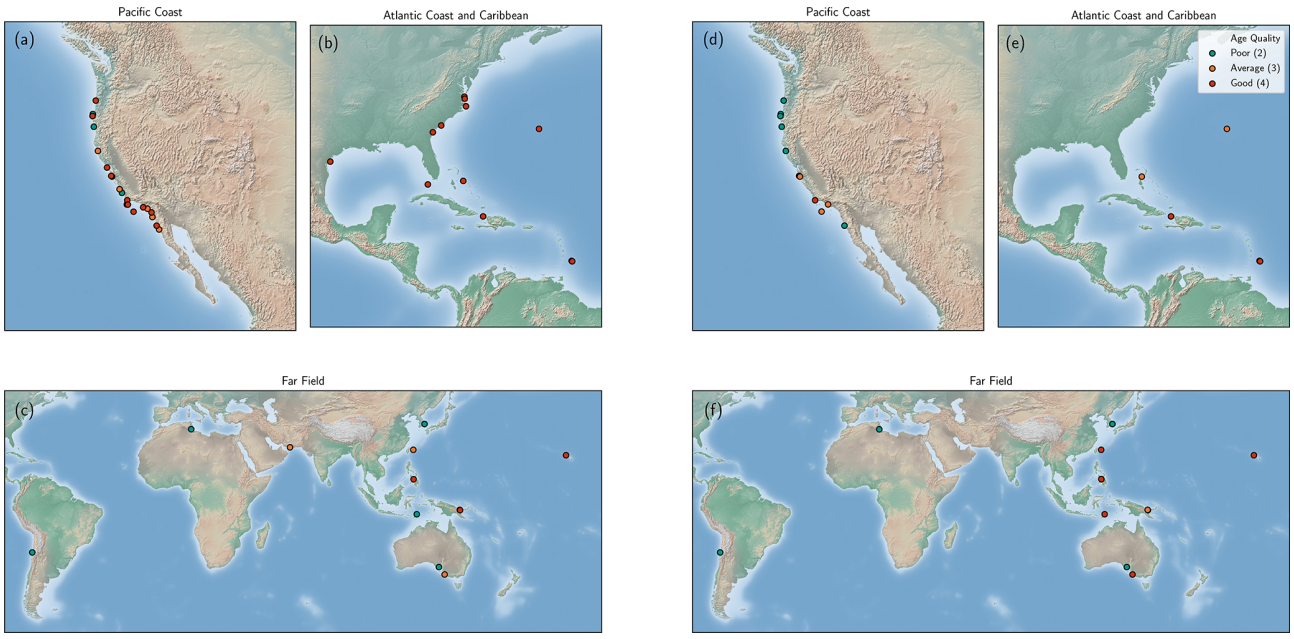

Figure 7. MIS 5a **(a–c)** and MIS 5c **(d–f)** sea level indicator chronology quality ratings atop the Matplotlib Basemap Shaded Relief map (Hunter, 2007). For the five Iranian subsites we plotted the lowest quality ratings of those listed in Tables 1 and 2.

wide and continuous surface, covered in sediment of up to 2 m thick; the T3b terrace, with a shoreline angle mapped at 17–22 m a.p.s.l. (Fig. 3), is a narrow, lower bench of the T3 terrace, separated from the upper bench by a gently sloping riser, which in places makes it difficult to distinguish the two platforms. A total of 16 optically stimulated luminescence ages assign the T2 terrace to MIS 5a (Choi et al., 2003; see the literature referenced in table 2 of Choi et al., 2008; see Fig. 4); 8 OSL ages and 2 paleomagnetic ages assign the T3b terrace to MIS 5c (Choi et al., 2003, 2008; see literature referenced in table 3 of Choi et al., 2008; see Fig. 5).

5.3.4 Pamilacan Island, Philippines

Ringor et al. (2004) mapped the coral reef terraces on Pamilacan Island, for which four uranium-series ages on corals have assigned the unnamed broad terrace, with a shoreline angle mapped at 6 m a.p.s.l., and the more narrow and poorly developed terrace (also unnamed), with a shoreline angle mapped at 13 m a.p.s.l., to MIS 5a and 5c, respectively.

5.3.5 Panglao Island, Philippines

Omura et al. (2004) mapped the coral reef terraces found along Panglao Island. The lowest well-developed terrace is mapped at 5 m a.p.s.l. (Fig. 3) and is composed of two geomorphic units. The lower unit contains one uranium-series age on *Porites* which dates to late MIS 5e. Four uranium-series ages on *Platygyra ryukyuensis* assign the upper terrace, of which the inner margin is mapped at 5 m a.p.s.l., to MIS 5c (Fig. 5).

5.3.6 Tewai and Kwambu sections, Huon Peninsula

Chappell (1974) first mapped the emergent coral reef terraces along the northern coast of the Huon Peninsula, of which we focus on the well-preserved, laterally tilted Va and VIa terraces. A total of 11 uranium-series ages on corals and mollusks assign these terraces to MIS 5a and 5c (Veeh and Chappell, 1970; Chappell, 1974; Esat et al., 1999; Cutler et al., 2003; Figs. 4 and 5). Chappell and Shackleton (1986) reported the reef crest elevations of the Va and VIa reef terraces to be 260 and 338 m a.p.s.l. at the Tewai section and 117 and 160 m a.p.s.l. at the Kwambu section (Figs. 2 and 3). Chappell et al. (1996) reconciled Huon Peninsula terrace highstands with oxygen isotope records for the interval spanning 70–30 ka.

5.3.7 Hateruma Island, Japan

Ota and Hori (1980) proposed an initial chronology for the six lowest Quaternary terraces around Hateruma Island following early mapping efforts discussed in Ota and Omura (1992). Omura (1984) published four uranium-series ages on corals that assigned terraces V and IV to MIS 5a and 5c, respectively (Figs. 4 and 5). The updated elevation surveys of Ota and Omura (1992) mapped the maximum height of the terraces V and IV at 23 and 30 m a.p.s.l., respectively (Figs. 2 and 3).

5.3.8 Atauro Island, East Timor

The lowest two coral reef terraces of Atauro Island, termed 1a and 1b, are mapped at inner-edge elevations of 20 and 36 m a.p.s.l., respectively (see the literature discussed in Chappell and Veeh, 1978; Figs. 2 and 3). Two uranium-series ages on corals have assigned terrace 1b to MIS 5c (Fig. 5). While no radiometric ages exist for Terrace 1a, Chappell and Veeh (1978) used the position of this terrace on age–height plots to infer an age of MIS 5a (Fig. 4).

5.3.9 Spencer Gulf, Australia

Hails et al. (1984) utilized sediment cores and sonar to study shallow-water stratigraphy in the Spencer Gulf, for which we focus on the Lowly Point and False Bay formations. The Lowly Point and False Bay formations occur at water depths exceeding 14 and 8 m b.p.s.l., respectively (Figs. 2 and 3). No radiometric ages exist for either formation; the stratigraphic position of the Lowly Point and False Bay formations between the MIS 5e-aged Mambray Formation and the Holocene age Germein Formation (see the literature discussed in Hails et al., 1984), along with the extent to which the depositional events flooded Spencer Gulf, supports age assignments of MIS 5a and 5c (Figs. 4 and 5).

5.3.10 Robe Range, Australia

Sprigg (1952) first mapped the eolianite barrier–shoreline complex of the Robe Range, for which we focus on the Robe II and III units. The barrier shoreline is fragmented in some regions and more extensively preserved in areas with higher uplift rates (Murray-Wallace, 2018). Schwebel (1984) reported a barrier shoreline elevation of −6–2 m a.p.s.l. for the Robe II unit (Fig. 2); Murray-Wallace (2002) reported the shoreline elevation of Robe III as 2 m b.p.s.l., revised upward from an earlier reported elevation of 15–8 m b.p.s.l. (Schwebel, 1984) (Fig. 3). Comparison between the local stratigraphy and established deep-ocean oxygen isotope records assigns the Robe II and Robe III shorelines to MIS 5a and 5c (Schwebel, 1984). Calibrated amino acid ratios on the Robe III barrier are numerically indistinguishable from the adjacent Robe II barrier, which hosts numerical AAR ages that fall within MIS 5a, though the authors note that the AAR method is not able to distinguish specific MISs (Blakemore et al., 2015). Based on anomalously young luminescence ages, debate exists in the literature as to whether the Robe II barrier records a true interglacial sea level highstand or formed as a result of local processes (Huntley et al., 1993a; see the literature discussed in Huntley et al., 1993a; Banerjee et al., 2003; Murray-Wallace, 2018). We include Robe II in the database as an MIS 5a indicator for completeness, along with the associated anomalously young ages (Fig. 4). Four luminescence ages, in conjunction with the stratigraphic position of the Robe III unit, support an age assignment of MIS 5c (Huntley et al., 1993b, 1994; Huntley and Prescott, 2001; Banerjee et al., 2003; Fig. 5).

5.3.11 Makran Subduction Zone, Iran (Lipar, Ramin, Gurdim, and Jask sites)

Harrison (1941) first documented the marine terraces along the Makran subduction zone of Iran; subsequent authors extended the initial mapping, documenting the differential uplift and lateral tilting of the terraces (Page et al., 1979; Reyss et al., 1998; Normand et al., 2019). Normand et al. (2019) revisited the terraces and provided updated elevations for the terraces found at the Lipar, Ramin, Gurdim, and Jask sites. The majority of the T1 terraces, dated with three optically stimulated luminescence ages and a single uranium-series age to MIS 5a (Fig. 4), have a shoreline angle mapped at 2 m b.p.s.l. to 65 m a.p.s.l. (Normand et al., 2019; Fig. 2). Normand et al. (2019) expanded on the history of the T1 terrace at the Ramin site, which hosts two luminescence samples dated to MIS 5e and 5a, respectively, concluding that the chronology implies a reoccupation of the T1 terrace during multiple sea level highstands (Fig. 4). The Lipar site also contains a T2 terrace mapped at 45 m a.p.s.l. (Fig. 2), which hosts a luminescence sample dated to MIS 5a (Fig. 4).

5.3.12 The Gulf of Gabes, Tunisia

Gzam et al. (2016) utilized high-precision echo sounders to map two submerged beach ridges, with peak elevations of 8 and 19 m b.p.s.l. (Figs. 2 and 3). From their analysis of biocalcarenite development, the authors concluded that the ridge formation could indicate a rapid sea level transgression, which, along with the stratigraphic position of the 8 and 19 m ridges, supported their respective age assignments of MIS 5a and 5c (Figs. 4 and 5). At present, no radiometric ages exist for these beach ridges.

5.3.13 Summary

Sea level indicators in the far field encompass marine terraces, coral reef terraces, and both marine- and terrestrial-limiting indicators (shallow-water facies and beach ridges, respectively), which have quality ratings between average (3) and rejected (0) (Fig. 6c and f and Tables 1 and 2). As with the previous two regions, we used IMCalc to quantify the indicative meaning of each relative sea level indicator in the absence of reported modern analog data (WALIS RSL IDs 3520–3537, 3557–3562, 3982; Lorscheid and Rovere, 2019). Most primary references do not report a clear reference datum, which limits the maximum quality rating to average (3). An average (3) rating for a coral reef terrace typically reflects both a precise measurement and a narrow indicative range (less than ~ 2 m) as calculated by IMCalc (as for MIS 5a and 5c indicators at Pamilacan Island and Hateruma Island and the MIS 5c indicator at Panglao Island). In contrast, as

marine terraces typically have larger indicative ranges, an average (3) quality rating necessitates a precise elevation measurement (e.g., the MIS 5a and 5c indicators at Daebo–Gori region and the MIS 5a indicators at Lipar and Gurdim). Poor ratings (2) for marine and coral reef terraces arise from imprecise measurements intrinsic to survey methods such as altimeters and topographic maps or from not reporting measurement uncertainty (such as the MIS 5a and 5c indicators at Bahía Inglesa, Oahu, Atauro Island, Tewai section, and Kwambu section and MIS 5a indicators at Ramin and Jask). All sites in Tunisia and Australia receive rejected (0) quality ratings because they only provide minimum and maximum limiting constraints on paleo-sea level. In summary, we advocate for applying modern measurement methods (with more precise error estimates) to marine and coral reef terraces with present quality ratings of average (3) and poor (2) to refine indicative meaning.

The far-field chronologies' quality ratings range from good (4) to poor (2) (Fig. 7c and f and Tables 1 and 2). Good quality ratings (4) are conferred through two avenues: first, from uranium-series ages on skeletal coral reef terraces that fall within a single MIS (such as for MIS 5a and 5c indicators at Oahu and Pamilacan Island; the MIS 5a indicator at Tewai section; and the MIS 5c indicators at Panglao Island, Hateruma Island, and Atauro Island) and second, from replicated high-precision luminescence ages (on MIS 5a indicators at Lipar, Gurdim, and Jask and the MIS 5c indicator at Robe Range). Average ratings (3) reflect chronologies where the age uncertainty exceeds a single MIS, either through uranium-series dating on coral (as for the MIS 5a and 5c Kwambu section indicators and the MIS 5a Hateruma Island indicator), luminescence dating (the MIS 5a Ramin indicator), or AAR dating (the MIS 5a Robe Range indicator). A poor rating (2) may reflect one of a number of relative dating methods used, including minimum limiting luminescence and paleomagnetic ages (MIS 5a and 5c Daebo–Gori indicators), terrace counting (indicators at MIS 5a and 5c Bahía Inglesa, Zarat, Zerkine, and Spencer Gulf; MIS 5a indicators at Bsissi, Ghannouche, Teboulbou, and Kettana; and the MIS 5c Tewai section indicator), and other correlation methods (MIS 5a Atauro Island indicator). As above, we advocate revisiting sites with quality ratings of average (3) or poor (2) to better constrain the age uncertainty.

6 Data availability

The database detailed in this study is available at https://doi.org/10.5281/zenodo.5021306 (Thompson and Creveling, 2021). The content at this link was exported from the WALIS database interface on 23 June 2021. A summary of these WALIS data can be found in Tables 1 and 2 of this paper. A description of each data field in the database is contained at this link: https://doi.org/10.5281/zenodo.3961543 (Rovere et al., 2020). More information on the World Atlas of Last Interglacial Shorelines can be found here: https://warmcoasts.eu/world-atlas.html (last access: 23 June 2021). Users of this database are encouraged to cite the primary literature sources as well as this article.

7 Review of research themes on MIS 5a and 5c RSL indicators and future research directions

The global database of sea level indicators dated (or assigned) to MIS 5a and 5c presented in this paper reasonably covers the Pacific coast of North America (18 field sites) and the Atlantic coast of North America and the Caribbean (9 field sites) and more sparsely covers the remaining globe (12 field sites). The broad geographic spread of the data allows for an increasingly resolved reconstruction of MIS 5a and 5c GMSL sea level, with especially good coverage in the near field of the North American ice sheets. Future efforts could expand this database by including additional indicators reported outside of North America, particularly those reported in non-English-language journals.

Two complementary research themes rely upon MIS 5 relative sea level indicators with unequivocal substage chronology and robust elevation data. One focus leverages the spatial variation in reconstructions of *local* MIS 5a and 5c RSL elevations to constrain global geophysical models for glacial isostatic adjustment and, hence, to refine estimates of substage global mean sea level (GMSL; e.g., Lambeck and Chappell, 2001; Potter and Lambeck, 2004; Muhs et al., 2012; Creveling et al., 2017). The other focus deduces regional rates of tectonic motion from the vertical displacement of (MIS 5e) RSL indicators from the sea level at which they formed (e.g., Matthews, 1973; Chappell, 1974; Muhs et al., 1990, 1992b; Simms et al., 2016). Numerous field and numerical analyses highlight the entanglement of these themes. Robust efforts to deduce MIS 5a and 5c GMSL from misfit analyses between field observational data and GIA models necessitate a quantitative correction for a site's tectonic uplift history (Creveling et al., 2015; Simms et al., 2016). Inasmuch as a vertical tectonic uplift correction requires a robust paleo-sea level reference datum, this reference datum should reflect the estimates of interstadial GMSL *and* melt-induced spatial variations in local sea level from glacial isostatic adjustment models (Creveling et al., 2015; Simms et al., 2016). Advances in each research theme enrich the other, and both rely upon RSL indicators with high-quality elevation measurements and substage-resolution chronology.

Tectonic uplift-corrected RSL indicators in the near-to-intermediate field of the North American ice complex display distinct geographic trends arising from glacial isostatic adjustment (Potter and Lambeck, 2004; Simms et al., 2016). North American Atlantic coast and Caribbean MIS 5a highstand elevations display a north-to-south latitudinal gradient that decreases by ∼30 m elevation (Cronin et al., 1981; Szabo, 1985; Bard et al., 1990; Cutler et al., 2003; Potter

et al., 2004; Wehmiller et al., 2004; Parham et al., 2013). Potter and Lambeck (2004) demonstrated that this trend reflects the glacioisostatic disequilibrium imposed by the forebulge of the Laurentide ice sheet. After correcting Atlantic coast and Caribbean RSL inferences for glacioisostasy, Potter and Lambeck (2004) concluded that MIS 5a GMSL peaked ~ -28 m below present (with a similar value for MIS 5c). Potter and Lambeck (2004) predicted magnitudes, though narrower bounds, on MIS 5a and 5c substage GMSL that were broadly consistent with Lambeck and Chappell (2001), who reconstructed GMSL of 23–37 and 18–30 m below present, respectively, from Huon Peninsula coral reef terraces. In contrast, tectonic uplift- and GIA-corrected MIS 5a and MIS 5c RSL indicators along the Pacific coast of the US and Mexico reveal an opposing latitudinal gradient in local high-stand elevations from that observed on the North American Atlantic coast and Caribbean (Simms et al., 2016). On the basis of the North American Pacific coast geographic gradient, Simms et al. (2016) concluded that MIS 5a and 5c peak GMSL reached up to ~ -15 and ~ -10 m below present sea level, a conclusion in agreement with that of Muhs et al. (2012), who reconstructed peak GMSL elevations of -16 and -9 m during MIS 5a and MIS 5c, respectively, based on tectonic uplift- and GIA-corrected RSL indicators at San Nicolas Island, California; the Florida Keys; and Barbados.

The opposing latitudinal gradients in MIS 5a and 5c peak highstand elevations imposed by the peripheral bulge of the North American ice complex do not find reconciliation with conventional "1-D" glacial isostatic adjustment models that assume a depth-varying but laterally homogenous viscoelastic structure (Creveling et al., 2017). Notably, embedding an upper-mantle viscosity in GIA models to reconcile the high-stand latitudinal gradient from one geographic region (i.e., the Pacific or Atlantic coast of North America) exacerbates the misfit of GIA predictions to the RSL indicators of the other region. Hence, GIA analyses that focus on a regional subset of global data produce GMSL estimates with systematic errors (hence the conflicting GMSL predictions of Potter and Lambeck, 2004, vs. Simms et al., 2016). Creveling et al. (2017) promoted the adoption of a sensitivity analysis between globally distributed RSL indicators and GIA predictions that adopt viscosity models that honor the complexity in (North American) upper-mantle viscosity. The resulting analytical workflow, applied to an unfiltered compendium of MIS 5a and 5c RSL indicators, yielded peak GMSL bounds of -18 ± 1 and -20 ± 1 m for MIS 5a and MIS 5c, respectively; notably, repeating this sensitivity analysis on an RSL database filtered to include only those with high-quality (predominately uranium-series) chronology widened these bounds to -22 ± 1 and -24 ± 2 m, respectively (Creveling et al., 2017).

Continued refinement of MIS 5a and 5c peak GMSL and regional rates of Quaternary vertical tectonic uplift remains within reach. First, numerical models for glacial isostatic adjustment that adopt "3-D" solid earth models with depth-varying and laterally homogenous viscoelastic structure promise to reconcile observed spatial gradients in RSL highstands and GIA model predictions (e.g., Latychev et al., 2005; Clark et al., 2019). Such numerical advancements offer the possibility of refining GMSL estimates in the absence of further field data collection. Second, the quality ratings conferred above motivate the strategic re-surveying of a subset of MIS 5a and 5c field observations (see Sect. 5.1.19, 5.2.10, and 5.3.13) in order that each site conforms to the uniform approach to establishing indicator elevation and age defined by the World Atlas of Last Interglacial Sea Level (e.g, Rovere et al., 2016). The re-sampling and/or re-analysis of geochronological material may also refine the numerical ages adopted for the World Atlas of Last Interglacial Sea Level (e.g, Rovere et al., 2016). Importantly, this retroactive translation of MIS 5a and 5c RSL observations to rigorous sea level index points (sensu Hijma et al., 2015) offers the paired promise of refining predictions of contemporaneous global mean sea level and vertical tectonic motion and the standardization of efforts to complete these research foci. Third, the proliferation of airborne lidar data can offer geoscientists a fresh perspective on the quantity and spatial relationships of purported terrace platforms (Bowles and Cowgill, 2012) that, once ground-truthed, may confer confidence in or contradict chronologies developed from terrace-counting methods. In practice, simultaneous efforts to enact all three practices will enrich conclusions about MIS 5a and 5c GMSL bounds and the accompanying tectonic displacement of these RSL indicators.

Author contributions. SBT assumed primary responsibility for all entries into the WALIS database and the illustration of these data. SBT extended the literature review of MIS 5a and 5c indicators beyond that reported in Creveling et al. (2017). SBT and JRC contributed equally to the structure and writing of the manuscript.

Competing interests. The authors declare that they have no conflict of interest.

Disclaimer. Publisher's note: Copernicus Publications remains neutral with regard to jurisdictional claims in published maps and institutional affiliations.

Special issue statement. This article is part of the special issue "WALIS – the World Atlas of Last Interglacial Shorelines". It is not associated with a conference.

Acknowledgements. The data presented in this publication were compiled in WALIS, a sea level database interface, developed with funding from the ERC Starting Grant "WARMCOASTS" (ERC-StG-802414), in collaboration with the PALSEA (PAGES/INQUA)

working group. The database structure was designed by Alesseo Rovere, Deirdre Ryan, Thomas Lorscheid, Andrea Dutton, Peter Chutcharavan, Dominik Brill, Nathan Jankowski, Daniela Mueller, Melanie Bartz, Evan Gowan, and Kim Cohen. The authors wish to thank Daniel Muhs for clarifying innumerable aspects of MIS 5a and 5c field observations and geochronological caveats over many years of conversation and Colin Murray-Wallace, one anonymous referee, editor Deirdre Ryan, and Alessio Rovere for constructive comments on manuscript drafts and database entries.

Review statement. This paper was edited by Deirdre Ryan and reviewed by Colin V. Murray-Wallace and one anonymous referee.

References

Adams, J.: Active deformation of the Pacific Northwest Continental Margin, Tectonics, 3, 449–472, https://doi.org/10.1029/TC003i004p00449, 1984.

Addicott, W. O. and Emerson, W. K.: Late Pleistocene Invertebrates from Punta Cabras, Baja California, Mexico, Am. Mus. Novit., 1925, 1–34, 1959.

Alexander, C. S.: The marine and stream terraces of the Capitola-Watsonville area, University of California Publications in Geology, 1953.

Allen, C. R., Silver, L. T., and Stehli, F. G.: Agua Blanca fault – A major transverse structure of northern Baja California, Mexico, Geol. Soc. Am. Bull., 71, 457–482, https://doi.org/10.1130/0016-7606(1960)71[467:ABFMTS]2.0.CO;2, 1960.

Banerjee, D., Hildebrand, A. N., Murray-Wallace, C. V., Bourman, R. P., Brooke, B. P., and Blair, M.: New quartz SAR-OSL ages from the stranded beach dune sequence in south-east South Australia, Quaternary Sci. Rev., 22, 1019–1025, 2003.

Bard, E., Hamelin, B., and Fairbanks, R. G.: U-Th ages obtained by mass spectrometry in corals from Barbados: Sea level during the past 130,000 years, Nature, 346, 456–458, 1990.

Barnes, J. W., Lang, E. J., and Potratz, H. A.: Ratio of ionium to uranium in coral limestone, Science, 124, 175–176, 1956.

Bender, M. L., Fairbanks, R. G., Taylor, F. W., Matthews, R. K., Goddard, J. G., and Broecker, W. S.: Uranium-series dating of the Pleistocene reef tracts of Barbados, West Indies, Bull. Geol. Soc. Am., 90, 577–594, https://doi.org/10.1130/0016-7606(1979)90<577:UDOTPR>2.0.CO;2, 1979.

Berger, G. W. and Hanson, K. L.: Thermoluminescence Ages of Estuarine Deposits Associated With Quaternary Marine Terraces, South-Central California, in: Quaternary coasts of the United States, edited by: Fletcher, C. H. and Wehmiller, J. F., SEPM Society for Sedimentary Geology, Tulsa, Oklahoma, USA, 303–308, 1992.

Birkeland, P. W.: Late Quaternary Eustatic Sea-Level Changes along the Malibu Coast, Los Angeles County, California, J. Geol., 80, 432–448, https://doi.org/10.1086/627765, 1972.

Blakemore, A. G., Murray-Wallace, C. V., Westaway, K. E., and Lachlan, T. J.: Aminostratigraphy and sea-level history of the Pleistocene Bridgewater Formation, Mount Gambier region, southern Australia, Aust. J. Earth Sci., 62, 151–169, 2015.

Bowles, C. J. and Cowgill, E.: Discovering marine terraces using airborne LiDAR along the Mendocino-Sonoma coast, northern California, Geosphere, 8, 386–402, https://doi.org/10.1130/GES00702.1, 2012.

Bradley, W. C. and Addicott, W. O.: Age of First Marine Terrace Near Santa Cruz, California, Geol. Soc. Am. Bull., 79, 1203–1210, https://doi.org/10.1130/0016-7606(1968)79[1203:AOFMTN]2.0.CO;2, 1968.

Bradley, W. C. and Griggs, G. B.: Form, genesis, and deformation of central California wave-cut platforms, Bull. Geol. Soc. Am., 87, 433–449, https://doi.org/10.1130/0016-7606(1976)87<433:FGADOC>2.0.CO;2, 1976.

Bretz, J. H.: Bermuda: A Partially Drowned, Late Mature, Pleistocene Karst, Bull. Geol. Soc. Am., 71, 1729–1754, 1960.

Broecker, W. S. and Thurber, D. L.: Uranium-series dating of corals and oolites from Bahaman and Florida Key limestones, Science, 149, 58–60, 1965.

Broecker, W. S., Thurber, D. L., Goddard, J., Ku, T. L., Matthews, R. K., and Mesolella, K. J.: Milankovitch hypothesis supported by precise dating of coral reefs and deep-sea sediments, Science, 159, 297–300, https://doi.org/10.1126/science.159.3812.297, 1968.

Carter, G. F.: Pleistocene man at San Diego, Johns Hopkins Press, Baltimore, 400, 1957.

Chappell, J.: Geology of coral terraces, Huon Peninsula, New Guinea: A study of Quaternary tectonic movements and sea-level changes, Bull. Geol. Soc. Am., 85, 553–570, https://doi.org/10.1130/0016-7606(1975)86<1482:GOCTHP>2.0.CO;2, 1974.

Chappell, J. and Shackleton, N. J.: Oxygen isotopes and sea level, Nature, 324, 137–140, https://doi.org/10.1038/324137a0, 1986.

Chappell, J. and Veeh, H. H.: Late Quaternary tectonic movements and sea-level changes at Timor and Atauro Island, Bull. Geol. Soc. Am., 89, 356–368, https://doi.org/10.1130/0016-7606(1978)89<356:LQTMAS>2.0.CO;2, 1978.

Chappell, J., Omura, A., Esat, T., McCulloch, M., Pandolfi, J., Ota, Y., and Pillans, B.: Reconciliation of late Quaternary sea levels derived from coral terraces at Huon Peninsula with deep sea oxygen isotope records, Earth Planet. Sc. Lett., 141, 227–236, 1996.

Choi, J. H., Murray, A. S., Jain, M., Cheong, C. S., and Chang, H. W.: Luminescence dating of well-sorted marine terrace sediments on the southeastern coast of Korea, Quaternary Sci. Rev., 22, 407–421, https://doi.org/10.1016/S0277-3791(02)00136-1, 2003.

Choi, S. J., Merritts, D. J., and Ota, Y.: Elevations and ages of marine terraces and late Quaternary rock uplift in southeastern Korea, J. Geophys. Res.-Sol. Ea., 113, 1–15, https://doi.org/10.1029/2007JB005260, 2008.

Chutcharavan, P. M. and Dutton, A.: A global compilation of U-series-dated fossil coral sea-level indicators for the Last Interglacial period (Marine Isotope Stage 5e), Earth Syst. Sci. Data, 13, 3155–3178, https://doi.org/10.5194/essd-13-3155-2021, 2021.

Clark, J., Mitrovica, J. X., and Latychev, K.: Glacial isostatic adjustment in central Cascadia: Insights from three-dimensional Earth modeling, Geology, 47, 295–298, https://doi.org/10.1130/G45566.1, 2019.

Creveling, J. R., Mitrovica, J. X., Hay, C. C., Austermann, J., and Kopp, R. E.: Revisiting tectonic corrections applied to Pleis-

tocene sea-level highstands, Quaternary Sci. Rev., 111, 72–80, 2015.

Creveling, J. R., Mitrovica, J. X., Clark, P. U., Waelbroeck, C., and Pico, T.: Predicted bounds on peak global mean sea level during marine isotope stages 5a and 5c, Quaternary Sci. Rev., 163, 193–208, https://doi.org/10.1016/j.quascirev.2017.03.003, 2017.

Cronin, T. M., Szabo, B. J., Ager, T. A., Hazel, J. E., and Owens, J. P.: Quaternary climates and sea levels of the U. S. Atlantic coastal plain, Science, 211, 233–240, https://doi.org/10.1126/science.211.4479.233, 1981.

Cutler, K. B., Edwards, R. L., Taylor, F. W., Cheng, H., Adkins, J., Gallup, C. D., Cutler, P. M., Burr, G. S., and Bloom, A. L.: Rapid sea-level fall and deep-ocean temperature change since the last interglacial period, Earth Planet. Sc. Lett., 206, 253–271, https://doi.org/10.1016/S0012-821X(02)01107-X, 2003.

Davis, W. M.: Glacial epochs of the Santa Monica Mountains, California, P. Natl. Acad. Sci. USA, 18, 659–665, https://doi.org/10.1073/pnas.18.11.659, 1932.

Dibblee Jr., T. W. and Ehrenspeck, H. E.: General geology of Santa Rosa Island, California, in: Contributions to the Geology of the Northern Channel Islands, Southern California, edited by: Weigand, P. W., Pacific Section American Association of Petroleum Geologists, Bakersfield, California, USA, 1998.

Dodge, R. E., Fairbanks, R. G., Benninger, L. K., and Maurrasse, F.: Pleistocene sea levels from raised coral reefs of Haiti, Science, 219, 1423–1425, https://doi.org/10.1126/science.219.4591.1423, 1983.

Duller, G. A. T.: Luminescence dating of Quaternary sediments: Recent advances, J. Quaternary Sci., 19, 183–192, https://doi.org/10.1002/jqs.809, 2004.

Dumas, B., Hoang, C. T., and Raffy, J.: Record of MIS 5 sea-level highstands based on U/Th dated coral terraces of Haiti, Quatern. Int., 145–146, 106–118, https://doi.org/10.1016/j.quaint.2005.07.010, 2006.

Dutton, A. and Lambeck, K.: Ice Volume and Sea Level During the Last Interglacial, Science, 216, 216–220, https://doi.org/10.1126/science.1205749, 2012.

Dutton, A., Carlson, A. E., Long, A. J., Milne, G. A., Clark, P. U., DeConto, R., Horton, B. P., Rahmstorf, S., and Raymo, M. E.: Sea-level rise due to polar ice-sheet mass loss during past warm periods, Science, 349, 6244, https://doi.org/10.1126/science.aaa4019, 2015.

Edwards, R. L., Cheng, H., Murrell, M. T., and Goldstein, S. J.: Protactinium-231 dating of carbonates by thermal ionization mass spectrometry: Implications for quaternary climate change, Science, 276, 782–786, https://doi.org/10.1126/science.276.5313.782, 1997.

Ellis, A. J.: Physiography, in: Geology and ground waters of the western part of San Diego County, California, U.S. Geol. Survey Water-Supply Paper, 446, 20–50, 1919.

Esat, T. M., McCulloch, M. T., Chappell, J., Pillans, B., and Omura, A.: Rapid fluctuations in sea level recorded at Huon Peninsula during the penultimate deglaciation, Science, 283, 197–201, https://doi.org/10.1126/science.283.5399.197, 1999.

Grant, L. B., Mueller, K. J., Gath, E. M., Cheng, H., Edwards, R. L., Munro, R., and Kennedy, G. L.: Late Quaternary uplift and earthquake potential of the San Joaquin Hills, southern Los Angeles basin, California, Geology, 27, 1031–1034, https://doi.org/10.1130/0091-7613(1999)027<1031:LQUAEP>2.3.CO;2, 1999.

Griggs, A. B.: Chromite-Bearing Sands of the Southern Part of the Coast of Oregon, Geological Survey Bulletin, 1944, 113–150, 1945.

Grove, K., Sklar, L. S., Scherer, A. M., Lee, G., and Davis, J.: Accelerating and spatially-varying crustal uplift and its geomorphic expression, San Andreas Fault zone north of San Francisco, California, Tectonophysics, 495, 256–268, https://doi.org/10.1016/j.tecto.2010.09.034, 2010.

Gzam, M., Mejdoub, N. El, and Jedoui, Y.: Late quaternary sea level changes of gabes coastal plain and shelf: Identification of the MIS 5c and MIS 5a onshore highstands, Southern Mediterranean, J. Earth Syst. Sci., 125, 13–28, https://doi.org/10.1007/s12040-015-0649-7, 2016.

Hails, J. R., Belperio, A. P., and Gostin, V. A.: Quaternary sea levels, northern Spencer Gulf, Australia, Mar. Geol., 61, 373–389, https://doi.org/10.1016/0025-3227(84)90175-0, 1984.

Hanks, T. C., Bucknam, R. C., Lajoie, K. R., and Wallace, R. E.: Modification of Wave-Cut and Faulting-Controlled Landforms, J. Geophys. Res., 89, 5771–5790, https://doi.org/10.1029/JB089iB07p05771, 1984.

Hanson, K. L., Lettis, W. R., Wesling, J. R., Kelson, K. I., and Mezger, L.: Quaternary marine terraces, south-central coastal California: implications for crustal deformation and coastal evolution, in: Quaternary coasts of the United States, edited by: Fletcher, C. H. and Wehmiller, J. F., 323–332, https://doi.org/10.2110/pec.92.48.0323, 1992.

Harmon, R. S., Mitterer, R. M., Kriausakul, N., Land, L. S., Schwarcz, H. P., Garrett, P., Larson, G. J., Leonard Vacher, H., and Rowe, M.: U-series and amino-acid racemization geochronology of Bermuda: Implications for eustatic sea-level fluctuation over the past 250,000 years, Palaeogeogr. Palaeocl., 44, 41–70, https://doi.org/10.1016/0031-0182(83)90004-4, 1983.

Harrison, J. V.: Coastal Makran: Discussion, Geogr. J., 97, 15, https://doi.org/10.2307/1787108, 1941.

Hays, J. D., Imbrie, J., and Shackleton, N. J.: Variations in the earth's orbit: Pacemaker of the ice ages, Science, 194, 1121–1132, https://doi.org/10.1126/science.194.4270.1121, 1976.

Hearty, P. J.: The geology of Eleuthera Island, Bahamas: A Rosetta Stone of quaternary stratigraphy and sea-level history, Quaternary Sci. Rev., 17, 333–355, https://doi.org/10.1016/S0277-3791(98)00046-8, 1998.

Hearty, P. J.: Revision of the late Pleistocene stratigraphy of Bermuda, Sediment. Geol., 153, 1–21, https://doi.org/10.1016/S0037-0738(02)00261-0, 2002.

Hearty, P. J. and Kaufman, D. S.: Whole-rock aminostratigraphy and Quaternary sea-level history of the Bahamas, Quaternary Res., 54, 163–173, https://doi.org/10.1006/qres.2000.2164, 2000.

Hearty, P. J., Vacher, H. L., and Mitterer, R. M.: Aminostratigraphy and ages of Pleistocene limestones of Bermuda, Geol. Soc. Am. Bull., 104, 471–480, https://doi.org/10.1130/0016-7606(1992)104<0471:AAAOPL>2.3.CO;2, 1992.

Hertlein, L. G. and Grant IV, U. S.: The Geology and Paleontology of the Marine Pliocene of San Diego, California, Memoirs of the San Diego Society of Natural History, 2, 15–20, 1944.

Hijma, M. P., Engelhart, S. E., Törnqvist, T. E., Horton, B. P., Hu, P., and Hill, D. F.: A protocol for a geological sea-level database, in: Handbook of Sea-Level Research, edited by: Shennan, I., Long, A. J., and Horton, B. P., 536–556, Wiley, Germany, 2015.

Hunter, J. D.: Matplotlib: A 2D Graphics Environment, Comput. Sci. Eng., 9, 90–95, https://doi.org/10.1109/MCSE.2007.55, 2007.

Huntley, D. J. and Prescott, J. R.: Improved methodology and new thermoluminescence ages for the dune sequence in south-east South Australia. Quaternary Sci. Rev., 20, 687–699, 2001.

Huntley, D. J., Hutton, J. T., and Prescott, J. R.: The stranded beach-dune sequence of south-east South Australia: A test of thermoluminescence dating, 0–800 ka. Quaternary Sci. Rev., 12, 1–20, 1993a.

Huntley, D. J., Hutton, J. T., and Prescott, J. R.: Optical dating using inclusions within quartz grains, Geology, 21, 1087–1090, 1993b.

Huntley D. J., Hutton J. T., and Prescott J. R.: Further thermoluminescence dates from the dune sequence in south-east of South Australia, Quaternary Sci. Rev., 13, 201–207, https://doi.org/10.1016/0277-3791(94)90025-6, 1994.

Johnson, D. L.: Beachrock (water-tablerock) on San Miguel Island, in: Geology of the Northern Channel Islands, edited by: Weaver, D. W., AAPG and SEPM Pacific, Los Angeles, California, USA, 1969.

Kelsey, H. M. and Bockheim, J. G.: Coastal landscape evolution as a function of eustasy and surface uplift rate, Cascadia margin, southern Oregon, Bull. Geol. Soc. Am., 106, 840–854, https://doi.org/10.1130/0016-7606(1994)106<0840:CLEAAF>2.3.CO;2, 1994.

Kelsey, H. M., Ticknor, R. L., Bockheim, J. G., and Mitchell, C. E.: Quaternary upper plate deformation in coastal Oregon, Bull. Geol. Soc. Am., 108, 843–860, https://doi.org/10.1130/0016-7606(1996)108<0843:QUPDIC>2.3.CO;2, 1996.

Kennedy, G. L., Lajoie, K. R., and Wehmiller, J. F.: Aminostratigraphy and faunal correlations of late Quaternary marine terraces, Pacific Coast, USA, Nature, 299, 545–547, https://doi.org/10.1038/299545a0, 1982.

Kennedy, G. L., Wehmiller, J. F., and Rockwell, T. K.: Paleoecology and paleozoogeography of late Pleistocene marine- terrace faunas of southwestern Santa Barbara County, California, in: Quaternary coasts of the United States, edited by: Fletcher, C. H. and Wehmiller, J. F., 343–361, https://doi.org/10.2110/pec.92.48.0343, 1992.

Kern, J. P.: Late Quaternary deformation of the Nestor terrace on the east side of Point Loma, San Diego, California, in: Studies on the geology and geologic hazards of the greater San Diego area, California, edited by: Ross, A. and Dowlen, R. J., San Diego Assoc. Geologists and Assoc. Engineering, San Diego, California, USA, 1973.

Kern, J. P.: Origin and history of upper Pleistocene marine terraces, San Diego, California, Bull. Geol. Soc. Am., 88, 1553–1566, https://doi.org/10.1130/0016-7606(1977)88<1553:OAHOUP>2.0.CO;2, 1977.

Kern, J. P. and Rockwell, T. K.: Chronology and deformation of Quaternary marine shorelines, San Diego County, California, in: Quaternary coasts of the United States, edited by: Fletcher, C. H. and Wehmiller, J. F., 377–382, https://doi.org/10.2110/pec.92.48.0377, 1992.

Kindler, P. and Hearty, P. J.: Carbonate petrography as an indicator of climate and sea-level changes: New data from Bahamian Quaternary units, Sedimentology, 43, 381–399, https://doi.org/10.1046/j.1365-3091.1996.d01-11.x, 1996.

Kopp, R. E., Simons, F. J., Mitrovica, J. X., Maloof, A. C., and Oppenheimer, M.: Probabilistic assessment of sea level during the last interglacial stage, Nature, 462, 863–867, https://doi.org/10.1038/nature08686, 2009.

Ku, T. L. and Kern, J. P.: Uranium-series age of the upper pleistocene Nestor Terrace, San Diego, California, Bull. Geol. Soc. Am., 85, 1713–1716, https://doi.org/10.1130/0016-7606(1974)85<1713:UAOTUP>2.0.CO;2, 1974.

Lambeck, K. and Chappell, J.: Sea level change through the last glacial cycle, Science, 292, 679–686, https://doi.org/10.1126/science.1059549, 2001.

Land, L. S., MacKenzie, F. T., and Gould, S. J.: Pleistocene history of Bermuda, Geol. Soc. Am. Bull., 78, 993–1006, https://doi.org/10.1130/0016-7606(1967)78[993:PHOB]2.0.CO;2, 1967.

Latychev, K., Mitrovica, J. X., Tromp, J., Tamisiea, M. E., Komatitsch, D., and Christara, C. C.: Glacial isostatic adjustment on 3-D earth models: A finite-volume formulation, Geophys. J. Int., 161, 421–444, 2005.

Lidz, B. H., Hine, A. C., Shinn, E. A., and Kindinger, J. L.: Multiple outer-reef tracts along the south Florida bank margin: outlier reefs, a new windward-margin model, Geology, 19, 115–118, https://doi.org/10.1130/0091-7613(1991)019<0115:MORTAT>2.3.CO;2, 1991.

Lindgren, W.: Notes on the geology of Baja California, Mexico, Proceedings of the California Academy of Sciences, 1, 173–196, 1889.

Lorscheid, T. and Rovere, A.: The indicative meaning calculator – quantification of paleo sea-level relationships by using global wave and tide datasets, Open Geospatial, Data Software and Standards, 4, 10, https://doi.org/10.1186/s40965-019-0069-8, 2019.

Ludwig, K. R., Muhs, D. R., Simmons, K. R., Halley, R. B., and Shinn, E. A.: Sea-level records at ∼80 ka from tectonically stable platforms: Florida and Bermuda, Geology, 24, 211–214, https://doi.org/10.1130/0091-7613(1996)024<0211:SLRAKF>2.3.CO;2, 1996.

Marquardt, C., Lavenu, A., Ortlieb, L., Godoy, E., and Comte, D.: Coastal neotectonics in Southern Central Andes: Uplift and deformation of marine terraces in Northern Chile (27° S), Tectonophysics, 394, 193–219, https://doi.org/10.1016/j.tecto.2004.07.059, 2004.

Matthews, R. K.: Relative elevationn of late Pleistocence high sea level stands: Barbados uplift rates and their implications, Quaternary Res., 3, 147–153, https://doi.org/10.1016/0033-5894(73)90061-6, 1973.

McInelly, G. W. and Kelsey, H. M.: Late Quaternary tectonic deformation in the Cape Arago-Bandon region of coastal Oregon as deduced from wave-cut platforms, J. Geophys. Res., 95, 6699–6713, https://doi.org/10.1029/JB095iB05p06699, 1990.

Merritts, D. and Bull, W. B.: Interpreting Quaternary uplift rates at the Mendocino triple junction, northern California, from uplifted marine terraces, Geology, 17, 1020–1024, https://doi.org/10.1130/0091-7613(1989)017<1020:IQURAT>2.3.CO;2, 1989.

Mesolella, K. J.: Zonation of Uplifted Pleistocene Coral Reefs on Barbados, West Indies, Science, 156, 638–640, 1967.

Mesolella, K. J., Matthews, R. K., Broecker, W. S., and Thurber, D. L.: The astronomical theory of climatic change: Barbados Data, J. Geol., 77, 250–274, https://doi.org/10.1086/627434, 1969.

Miller, G. H., Hollin, J. T., and Andrews, J. T.: Aminostratigraphy of UK Pleistocene deposits, Nature, 281, 539–543, https://doi.org/10.1038/281539a0, 1979.

Mirecki, J. E., Wehmillert, J. F., and Skinner, A. F.: Geochronology of Quaternary Coastal Plain Deposits, Southeastern Virginia, U.S.A., J. Coastal Res., 11, 1135–1144, 1995.

Mitterer, R. M.: Pleistocene stratigraphy in Southern Florida based on amino acid diagenesis in fossil mercenaria, Geology, 2, 425–428, https://doi.org/10.1130/0091-7613(1974)2<425:PSISFB>2.0.CO;2, 1974.

Mueller, K., Kier, G., Rockwell, T., and Jones, C. H.: Quaternary rift flank uplift of the Peninsular Ranges in Baja and southern California by removal of mantle lithosphere, Tectonics, 28, 1–17, https://doi.org/10.1029/2007TC002227, 2009.

Muhs, D. R., Kelsey, H. M., Miller, G. H., Kennedy, G. L., Whelan, J. F., and Mcinelly, G. W.: Age Estimates and Uplift Rates for Late Pleistocene Marine Terraces, J. Geophys. Res., 95, 6685–6698, https://doi.org/10.1029/JB095iB05p06685, 1990.

Muhs, D. R., Miller, G. H., Whelan, J. F., and Kennedy, G. L.: Aminostratigraphy and oxygen isotope stratigraphy of marine-terrace deposits, Palos Verdes Hills and San Pedro areas, Los Angeles County, California, in: Quaternary coasts of the United States, edited by: Fletcher, C. H. and Wehmiller, J. F., SEPM Society for Sedimentary Geology, Tulsa, Oklahoma, USA, 363–376, 1992a.

Muhs, D. R., Rockwell, T. K., and Kennedy, G. L.: Late quaternary uplift rates of marine terraces on the Pacific coast of North America, southern Oregon to Baja California sur, Quatern. Int., 15–16, 121–133, https://doi.org/10.1016/1040-6182(92)90041-Y, 1992b.

Muhs, D. R., Kennedy, G. L., and Rockwell, T. K.: Uranium-series ages of marine terrace corals from the Pacific coast of North America and implications for last-interglacial sea level history, Quaternary Res., 42, 72–87, https://doi.org/10.1006/qres.1994.1055, 1994.

Muhs, D. R., Simmons, K. R., and Steinke, B.: Timing and warmth of the Last Interglacial period: New U-series evidence from Hawaii and Bermuda and a new fossil compilation for North America, Quaternary Sci. Rev., 21, 1355–1383, https://doi.org/10.1016/S0277-3791(01)00114-7, 2002.

Muhs, D. R., Simmons, K. R., Kennedy, G. L., Ludwig, K. R., and Groves, L. T.: A cool eastern Pacific Ocean at the close of the Last Interglacial complex, Quaternary Sci. Rev., 25, 235–262, https://doi.org/10.1016/j.quascirev.2005.03.014 2006.

Muhs, D. R., Simmons, K. R., Schumann, R. R., Groves, L. T., Mitrovica, J. X., and Laurel, D. A.: Sea-level history during the Last Interglacial complex on San Nicolas Island, California: Implications for glacial isostatic adjustment processes, paleozoogeography and tectonics, Quaternary Sci. Rev., 37, 1–25, https://doi.org/10.1016/j.quascirev.2012.01.010, 2012.

Muhs, D. R., Simmons, K. R., Schumann, R. R., Groves, L. T., DeVogel, S. B., Minor, S. A., and Laurel, D. A.: Coastal tectonics on the eastern margin of the Pacific Rim: Late Quaternary sea-level history and uplift rates, Channel Islands National Park, California, USA, Quaternary Sci. Rev., 105, 209–238, https://doi.org/10.1016/j.quascirev.2014.09.017, 2014.

Murray-Wallace, C. V.: Pleistocene coastal stratigraphy, sea-level highstands and neotectonism of the southern Australian passive continental margin – A review, J. Quaternary Sci., 17, 469–489, https://doi.org/10.1002/jqs.717, 2002.

Murray-Wallace, C. V.: Quaternary history of the Coorong Coastal Plain, Southern Australia: An archive of environmental and global sea-level changes, Springer, Cham, 229, 2018.

Neumann, A. C. and Moore, W. S.: Sea level events and Pleistocene coral ages in the northern Bahamas, Quaternary Res., 5, 215–224, https://doi.org/10.1016/0033-5894(75)90024-1, 1975.

Newell, N. D.: Warm interstadial interval in Wisconsin stage of the Pleistocene, Science, 148, 1488, https://doi.org/10.1126/science.148.3676.1488, 1965.

Normand, R., Simpson, G., Herman, F., Biswas, R. H., Bahroudi, A., and Schneider, B.: Dating and morpho-stratigraphy of uplifted marine terraces in the Makran subduction zone (Iran), Earth Surf. Dynam., 7, 321–344, https://doi.org/10.5194/esurf-7-321-2019, 2019.

Omura, A.: Uranium-series Age of the Riukiu Limestone on Hateruma Island, Southwestern Ryukyus, Transactions and Proceedings of the Palaeontological Society of Japan, 415–426, https://doi.org/10.14825/prpsj1951.1984.135_415, 1984.

Omura, A., Maeda, Y., Kawana, T., Siringan, F. P., and Berdin, R. D.: U-series dates of Pleistocene corals and their implications to the paleo-sea levels and the vertical displacement in the Central Philippines, Quatern. Int., 115–116, 3–13, https://doi.org/10.1016/S1040-6182(03)00092-2, 2004.

Orr, P. C.: Prehistory of Santa Rosa Island, Santa Barbara Museum of Natural History, Santa Barbra, California, 1968.

Osmond, J. K., Carpenter, J. R., and Windom, H. L.: Th 230 /U 234 age of the Pleistocene corals and oolites of Florida, J. Geophys. Res., 70, 1843–1847, https://doi.org/10.1029/JZ070i008p01843, 1965.

Ota, Y. and Hori, N.: Late Quaternary tectonic movement of the Ryukyu Islands, Japan, The Quaternary Research (Daiyonki-kenkyu), 18, 221–240, https://doi.org/10.4116/jaqua.18.221, 1980.

Ota, Y. and Omura, A.: Contrasting styles and rates of tectonic uplift of coral reef terraces in the Ryukyu and Daito Islands, southwestern Japan, Quatern. Int., 15–16, 17–29, https://doi.org/10.1016/1040-6182(92)90033-X, 1992.

Page, W. D., Alt, J. N., Cluff, L. S., and Plafker, G.: Evidence for the recurrence of large-magnitude earthquake along the Makran coast of Iran and Pakistan, Tectonophysics, 52, 533–547, https://doi.org/10.1016/0040-1951(79)90269-5, 1979.

Parham, P. R., Riggs, S. R., Culver, S. J., Mallinson, D. J., Jack Rink, W., and Burdette, K.: Quaternary coastal lithofacies, sequence development and stratigraphy in a passive margin setting, North Carolina and Virginia, USA, Sedimentology, 60, 503–547, https://doi.org/10.1111/j.1365-3091.2012.01349.x, 2013.

Perg, L. A., Anderson, R. S., and Finkel, R. C.: Use of a new 10Be and 26Al inventory method to date marine terraces, Santa Cruz, California, USA, Geology, 29, 879–882, https://doi.org/10.1130/0091-7613(2001)029<0879:UOANBA>2.0.CO;2, 2001.

Pinter, N., Johns, B., Little, B., and Vestal, W. D.: Fault-related folding in California's Northern Channel Is-

lands documented by rapid-static GPS positioning, GSA Today, 11, 4–9, https://doi.org/10.1130/1052-5173(2001)011<0004:FRFICN>2.0.CO;2, 2001.

Potter, E. K. and Lambeck, K.: Reconciliation of sea-level observations in the Western North Atlantic during the last glacial cycle, Earth Planet. Sc. Lett., 217, 171–181, https://doi.org/10.1016/S0012-821X(03)00587-9, 2004.

Potter, E. K., Esat, T. M., Schellmann, G., Radtke, U., Lambeck, K., and McCulloch, M. T.: Suborbital-period sea-level oscillations during marine isotope substages 5a and 5c, Earth Planet. Sc. Lett., 225, 191–204, https://doi.org/10.1016/j.epsl.2004.05.034, 2004.

Railsback, L. B., Gibbard, P. L., Head, M. J., Voarintsoa, N. R. G., and Toucanne, S.: An optimized scheme of lettered marine isotope substages for the last 1.0 million years, and the climatostratigraphic nature of isotope stages and substages, Quaternary Sci. Rev., 111, 94–106, https://doi.org/10.1016/j.quascirev.2015.01.012, 2015.

Reyss, J. L., Pirazzoli, P. A., Haghipour, A., Hatté, C., and Fontugne, M.: Quaternary marine terraces and tectonic uplift rates on the south coast of Iran, Geol. Soc. Spec. Publ., 146, 225–237, https://doi.org/10.1144/GSL.SP.1999.146.01.13, 1998.

Ringor, C. L., Omura, A., and Maeda, Y.: Last Interglacial Terraces Sea Level in Southwest Changes Deduced Central from Coral Reef Terraces in Southwest Bohol, Central Philippines, Quaternary Res., 46, 401–416, https://doi.org/10.4116/jaqua.43.401, 2004.

Rockwell, T. K., Muhs, D. R., Kennedy, G. L., Hatch, M. E., Wilson, S. H., and Klinger, R. E.: Uranium-Series Ages, Faunal Correlations and Tectonic Deformation of Marine Terraces Within the Agua Blanca Fault Zone at Punta Banda, Northern Baja California, Mexico, Geologic Studies in Baja California, Pacific Section, Society of Economic Paleontologists and Mineralogists, Los Angeles, California, USA, 1–16, 1989.

Rockwell, T. K., Nolan, J., Johnson, D. L., and Patterson, R. H.: Age and Deformation of Marine Terraces Between Point Conception and Gaviota, Western Traverse Ranges, California, in: Quaternary coasts of the United States, edited by: Fletcher, C. H. and Wehmiller, J. F., SEPM Society for Sedimentary Geology, Tulsa, Oklahoma, USA, 333–341, 1992.

Rovere, A., Raymo, M. E., Vacchi, M., Lorscheid, T., Stocchi, P., Gómez-Pujol, L., Harris, D. L., Casella, E., O'Leary, M. J., and Hearty, P. J.: The analysis of Last Interglacial (MIS 5e) relative sea-level indicators: Reconstructing sea-level in a warmer world, Earth-Sci. Rev., 159, 404–427, https://doi.org/10.1016/j.earscirev.2016.06.006, 2016.

Rovere, A., Ryan, D., Murray-Wallace, C., Simms, A., Vacchi, M., Dutton, A., and Gowan, E.: Descriptions of database fields for the World Atlas of Last Interglacial Shorelines (WALIS) (Version 1,0), Zenodo, https://doi.org/10.5281/zenodo.3961544, 2020.

Schellmann, G. and Radtke, U.: A revised morpho- and chronostratigraphy of the Late and Middle Pleistocene coral reef terraces on Southern Barbados (West Indies), Earth-Sci Rev., 64, 157–187, 2004.

Schwebel, D. A.: Quaternary Stratigraphy and Sea-Level Variation in the Southeast of South Australia, in: Coastal Geomorphology in Australia, edited by: Thom, B. G., Academic Press, Sydney, 291–311, 1984.

Sherman, C. E., Fletcher, C. H., Rubin, K. H., Simmons, K. R., and Adey, W. H.: Sea-level and reef accretion history of Marine Oxygen Isotope Stage 7 and late Stage 5 based on age and facies of submerged late Pleistocene reefs, Oahu, Hawaii, Quaternary Res., 81, 138–150, https://doi.org/10.1016/j.yqres.2013.11.001, 2014.

Simms, A. R., DeWitt, R., Rodriguez, A. B., Lambeck, K., and Anderson, J. B.: Revisiting marine isotope stage 3 and 5a (MIS3-5a) sea levels within the northwestern Gulf of Mexico, Global Planet. Change, 66, 100–111, https://doi.org/10.1016/j.gloplacha.2008.03.014, 2009.

Simms, A. R., Rouby, H., and Lambeck, K.: Marine terraces and rates of vertical tectonic motion: The importance of glacio-isostatic adjustment along the Pacific coast of central North America, Bull. Geol. Soc. Am., 128, 81–93, https://doi.org/10.1130/B31299.1, 2016.

Sprigg, R. C.: Stranded Pleistocene sea beaches of South Australia and aspects of the theories of Milankovitch and Zeuner, Int. Geol. Congr. (XVI. II, GB, 1948), 1952.

Szabo, B. J.: Uranium-series dating of fossil corals from marine sediments of southeastern United States Atlantic Coastal Plain, Geol. Soc. Am. Bull., 96, 398–406, https://doi.org/10.1130/0016-7606(1985)96<398:UDOFCF>2.0.CO;2, 1985.

Szabo, B. J. and Rosholt, J. N.: Uranium-series dating of Pleistocene molluscan shells from southern California-An open system model, J. Geophys. Res., 74, 3253–3260, https://doi.org/10.1029/jb074i012p03253, 1969.

Thompson, S. and Creveling, J. R.: WALIS Spreadsheet Thompson Creveling, Zenodo, https://doi.org/10.5281/zenodo.5021306, 2021.

Thurber, D. L., Broecker, W. S., Blanchard, R. L., and Potratz, H. A.: Uranium-series ages of Pacific atoll coral, Science 149, 55–58, 1965.

Toscano, M. A. and Lundberg, J.: Submerged late pleistocene reefs on the tectonically-stable S. E. Florida margin: High-precision geochronology, stratigraphy, resolution of substage 5a sea-level elevation, and orbital forcing, Quaternary Sci. Rev., 18, 753–767, https://doi.org/10.1016/S0277-3791(98)00077-8, 1999.

Vacchi, M., Montefalcone, M., Schiaffino, C. F., Parravicini, V., Bianchi, C. N., Morri, C., and Ferrari, M.: Towards a predictive model to assess the natural position of the Posidonia oceanica seagrass meadows upper limit, Mar. Pollut. Bull., 83, 458–466, 2014.

Vacher, H. L. and Hearty, P.: History of stage 5 sea level in Bermuda: Review with new evidence of a brief rise to present sea level during Substage 5a, Quaternary Sci. Rev., 8, 159–168, https://doi.org/10.1016/0277-3791(89)90004-8, 1989.

Valensise, G. and Ward, S. N.: Long-term uplift of the Santa Cruz coastline in response to repeated earthquakes along the San Andreas Fault, B. Seismol. Soc. Am., 81, 1694–1704, 1991.

Vedder, J. G. and Norris, R. M.: Geology of San Nicolas Island California, US Geological Survey Professional Paper, 369, 65 pp., 1963.

Vedder, J. G., Yerkes, R. F., and Schoelhamer, J. E.: Geologic map of the San Joaquin Hills–San Juan Capistrano area, Orange County, California, U. S. Geological Survey Oil and Gas Investigations, Washington, D.C., USA, 1957.

Veeh, H. H. and Chappell, J.: Astronomical Theory of Climatic Change, Support from New Guinea, Science, 167, 862–865, https://doi.org/10.1126/science.167.3919.862, 1970.

Wehmiller, J. F., Simmons, K. R., Cheng, H., Edwards, R. L., Martin-McNaughton, J., York, L. L., Krantz, D. E., and Shen, C. C.: Uranium-series coral ages from the US Atlantic Coastal Plain-the "80 ka problem" revisited, Quatern. Int., 120, 3–14, https://doi.org/10.1016/j.quaint.2004.01.002, 2004.

Wehmiller, J. F., Brothers, L. L., Ramsey, K. W., Foster, D. S., and Mattheus, C. R.: Molluscan aminonstratigraphy of the US Mid-Atlantic Quaternary coastal system: implications for onshore-offshore correlation, paleochannel and barrier island evolution, and local late Quaternary sea-level history, Quat. Geochronol., 101177, https://doi.org/10.1016/j.quageo.2021.101177, in press, 2021a.

Wehmiller, J. F.: May 2nd: Summary of Amino Acid Racemization data and associated geochronological data, US Atlantic Coastal Plain, available at: https://arcg.is/1L0uyK, last access: 7 July 2021b.

Woodring, W. P., Brown, J. S., and Burbank, W. S.: Geology of the Republic of Haiti, Lord Baltimore Press, Port-au-Prince, Haiti, 631 pp., 1924.

Woodring, W. P., Bramlette, M. N., and Kew, W. S. W.: Geology and Paleontology of Palos Verdes Hills, California, U.S. Government Printing Office, District of Columbia, USA, 145, 1946.